Sustainable Materials and Technologies 41 (2024) e01008

Contents lists available at ScienceDirect

Sustainable Materials and Technologies

journal homepage: www.elsevier.com/locate/susmat

Developments and prospects of additive manufacturing for thermoelectric materials and technologies

Ahmad Baroutaji [a,*], Arun Arjunan [b,c], John Robinson [b,c], Mohamad Ramadan [d], Mohammad Ali Abdelkareem [e,f,g], Aaron Vance [b,c], Abul Arafat [b,c], Abdul-Ghani Olabi [a,e,f]

[a] School of Engineering and Technology, Aston University, Aston Triangle, Birmingham, B4 7ET, UK
[b] Additive Manufacturing of Functional Materials Research Group, Centre for Engineering Innovation and Research, University of Wolverhampton, Telford Innovation Campus, TF2 9NT, UK
[c] School of Engineering, Computing and Mathematical Sciences, University of Wolverhampton, WV1 1LY, UK
[d] School of Engineering, International University of Beirut, PO Box 146404, Beirut, Lebanon
[e] Sustainable Energy and Power Systems Research Centre, RISE, University of Sharjah, P.O. Box 27272, Sharjah, United Arab Emirates
[f] Dept. of Sustainable and Renewable Energy Engineering, University of Sharjah, P.O. Box 27272, Sharjah, United Arab Emirates
[g] Chemical Engineering Department, Minia University, Elminia, Egypt

ARTICLE INFO

Keywords:
Additive manufacturing
Thermoelectric
TEG
TEC
TEM
SLM
DIW
FDM

ABSTRACT

In view of the increased demand for electricity and the associated environmental and financial concerns, there is an urgent need to develop technological solutions that can improve the efficiency of engineering systems and processes. Thermoelectric (TE) technologies, with their capability of direct conversion of thermal energy into electrical energy, are promising technologies for green power generation through using them as energy harvesting devices for waste heat recovery in industrial processes and power generation systems.

To date, TE technologies are still not commercialized on a large scale due to various economic and technical obstacles. The majority of previous research on TE technologies concentrated on improving the TE properties, such as electronic transport and figure-of-merit, while limited attempts were made to identify the best material processing techniques or reduce the cost of manufacturing. Conventional Manufacturing (CM) of TE materials and devices is multi-stage, complex, labour-intensive, time-consuming, and has high energy requirements. Thus, manufacturing challenges are considered key contributors toward limited industrial adoption of TE technologies.

The rapid advent of advanced Additive Manufacturing (AM) processes, in recent years, caused dramatic changes in engineering design thinking and created opportunities to solve manufacturing challenges. With its significant capabilities, AM can be the route to address the shortcomings of CM of the thermoelectric technologies. In this regard, this paper presents an in-depth review of the literature studies on using AM technologies, such as selective laser melting, fused deposition modelling, direct ink writing, stereo lithography, etc., for manufacturing TE materials and devices. The benefits and challenges of each AM technology are discussed to identify their merits and the required future research. This paper demonstrates the role of AM in advancing green materials and technologies for solving some of the outstanding energy and environmental issues.

1. Introduction

The need to improve the efficiency of industrial processes and power generation systems is ever-urgent as global warming, caused by the heavy reliance on fossil fuels and the associated emissions of Greenhouse Gases (GHG), continues to impose serious challenges to our normal human life. Waste Heat Recovery (WHR) systems that recycle the wasted heat from industrial processes and power systems into practical use are one way to reduce waste energy and improve the efficiency of these systems. It is estimated that $\sim 20\% - 50\%$ of industrial energy consumption is not utilized usefully but conversely, it is discharged as waste heat into the environment [1]. Therefore, WHR systems can generate significant energy savings [2,3]. Among the various technologies, solid-state Thermoelectric Modules (TEMs), in their two configurations as Thermoelectric Generator (TEG) and Thermoelectric Cooler (TEC), have gained attention as environmentally friendly devices for harvesting waste heat through direct conversion of thermal energy into electricity and vice-versa [4]. TEMs are attractive because they are simple, silent,

* Corresponding author.

https://doi.org/10.1016/j.susmat.2024.e01008
Received 20 September 2023; Received in revised form 22 March 2024; Accepted 6 May 2024
Available online 6 June 2024

versatile, reliable, and have low maintenance requirements and mechanical failure probability as they have no moving parts [5]. TEG converts the thermal energy (heat) into electricity while TEC reversely converts electricity into thermal energy, i.e., generation of heat or cooling effects. TEGs can be used as waste heat harvesting systems in wireless sensor networks, wearable medical devices, hydrogen fuel cell, automobile engines, aerospace devices, and various industrial processes [6–8]. On the other side, TEC is a reliable, compactable, and silent refrigerator that provides many advantages over conventional compressor-based cooling systems [1]. For example, TEC does not need any exchange media such as a freon gas [9]. Also, TEC can be revised quickly from cooling to heating by changing the direction of the applied current. TECs are used for thermal management applications in medical, microchips and integrated circuits, optical equipment, aerospace and defence systems [10,11]. Some of the niche industrial applications of TEC are infrared detectors, temperature control of automotive seats, CPU coolers, and cooling of avionics and aviation components [12].

Despite their huge potential, the large-scale adoption of TEMs is hindered by many factors including manufacturing challenges, material costs, and low power conversion efficiency [7,13]. Many TE materials use germanium and/or tellurium which are expensive elements [5]. Conventional Manufacturing (CM) of TE materials and TEM is a complex multi-stage procedure, labour and energy intensive, time-consuming, requires complex equipment, not suitable for large-scale production, and can only fabricate simple planar geometry which has limited TE performance when the heat source has a complex shape [14–16]. The typical CM procedure of TEM starts with fabricating the TE material into pellets using a combination of processing techniques depending on the type of the material (further details are provided in Section 2.2). Following that, the pellets are diced and polished to form the different n-type and p-type TE legs. The legs are then joined to the interconnects (made of electrically conductive metal such as silver) which are connected to the substrates (made of electrically insulating but thermally conducting material such as ceramic). Solder or braze materials are used to connect the legs, interconnects, and substrates [17].

In recent years, AM, or Three Dimensional Printing (3DP), technologies enjoyed significant and rapid developments as well as wide adoption in many industrial sectors such as automotive [18], railway [19], aerospace [20], construction [21], biomedical [22–24], food [25,26], fashion and jewellery [27], and energy [28–30]. AM provides many benefits compared to CM. The distinct advantage of AM is its capability to create complex geometrical shapes rapidly. AM can be used to create new parts or to repair existing ones, from a wide range of materials such as metals, ceramic, polymers, and composites. AM accelerates the product development process as it allows rapid manufacturing of the product prototypes so engineers can estimate the performance and redesign the parts at the early stages of the development process.

AM not only add technical and economic benefits but also has many positive sustainability impacts. AM plays a key role in the transition to sustainable production and circular economy models. AM enables more efficient and flexible product and process design due to its significant design freedom. Such design freedom enables designing lightweight complex structures that may combine multiple functions together, thus reducing the number of required parts and simplifying the assembly process [31]. Due to its additive nature, AM maximizes the utilization of raw materials and minimizes material wastage making it a very resource-efficient manufacturing process [32]. Also, AM has great potential to be an important player in the models of on-demand, or make-to-order, product manufacturing and distributed manufacturing [33]. AM can mitigate supply chain costs and reduce transportation-related carbon dioxide (CO_2) emissions by on-demand production closer to the customers [34]. Additionally, AM can be used for on-demand production of replacement parts instead of maintaining an inventory of such parts thus reducing the inventory waste of unsold parts. Within the framework of circular economy, AM enables closed-loop material flows through reclaiming unused AM materials, such as resin and powder, or using recycled materials, from other products, as a feedstock for 3D printers [31]. For example, plastic bottles can be converted into 3D printable plastic filaments for FDM technology. In the same context, AM is attractive for maintenance and repair, and remanufacturing of high-value engineering products, thus contributing to extending the lifespan of such products. For instance, AM has been adopted for in-situ repairing of burners in gas turbines and blisks in jet engines [31]. Beside the above, most AM processes are low labour and fully automated processes and therefore they have very low health and safety risks.

With such versatile and advanced capabilities of AM, it is intuitive for the research community to consider AM as a potential solution to revolutionize the fabrication of TEM and to address the shortcomings of CM. Printing technologies, such as inkjet printing, aerosol jet printing, roll-to-roll printing, and screen printing, have been widely used for TEM fabrication [35]. The Technology Readiness Level (TRL) of TE technologies is relatively low, in the range of 3–5, meaning that they are still in the research and development phases and require significant developments to reach the deployment phase [36,37]. AM has the potential to fabricate traditional and emerging TE materials, thus paving the road to prepare innovative TEMs with advanced shapes and enhanced performance, contributing to advancing TE technologies. To estimate the potential of AM processes for TE devices and materials, it is important to systemically analyse their technical merits and challenges. To this end, the focus of this paper is to conduct a thorough literature review of the applications of 3DP technologies for TE materials and technologies. The paper is structured as follows. In Section 2, an overview of thermoelectricity and working principles of TEMs is provided. The application of the different AM technologies for fabricating TE materials and devices along with the main advantages and limitations are introduced in Section 3. Finally, the merits, challenges, and prospects of AM for TE materials are discussed in the conclusion section.

2. Overview of thermoelectricity

2.1. Working principles

TEMs, including TEG and TEC, are solid-state energy conversion devices that consist of multiple thermocouples, or thermoelectric elements, connected electrically in series and thermally in parallel [38]. Each thermocouple is composed of two dissimilar TE materials. TE materials are a class of semiconductors that directly convert thermal energy into electrical power and vice-versa [39]. According to the type of the primary charge carriers, TE materials can be either p-type or n-type. The p-type materials have holes (i.e., vacancies) as the primary carriers of the positive charge while n-type materials have electrons as the primary carriers of the negative charge. The working principles of the TE devices are based on three thermoelectric effects, including Seebeck, Peltier, and Thomson effects, that govern the energy conversion process between electricity and temperature gradient [7,40,41].

TEG produces electricity based on the Seebeck effect. The Seebeck effect states that when imposing a temperature gradient ($\Delta T = T_{hot} - T_{cold}$) on the junctions of a thermocouple (a pair of p- and n-type TE materials), a potential difference, i.e., electrical voltage (ΔV), is generated. The theory behind the Seebeck effect is that the applied ΔT induces the diffusion of charge carriers (electrons in the n-type material or holes in the p-type material) from the high temperature to the low temperature. The reason for this diffusion is that the added heat makes the charge carriers at the hot side more energetic than their counterparts at the cold side and thus they travel faster toward the cold side and accumulate there. The accumulation of the charge carriers at the cold side creates opposite charges at the ends of the TE materials, as shown in Fig. 1, resulting in a gradient in the concentration of charge carriers across the material and building up a potential difference between the hot and cold ends. The resulted electric potential starts to impede the diffusion process and eventually stops it when reaching an equilibrium

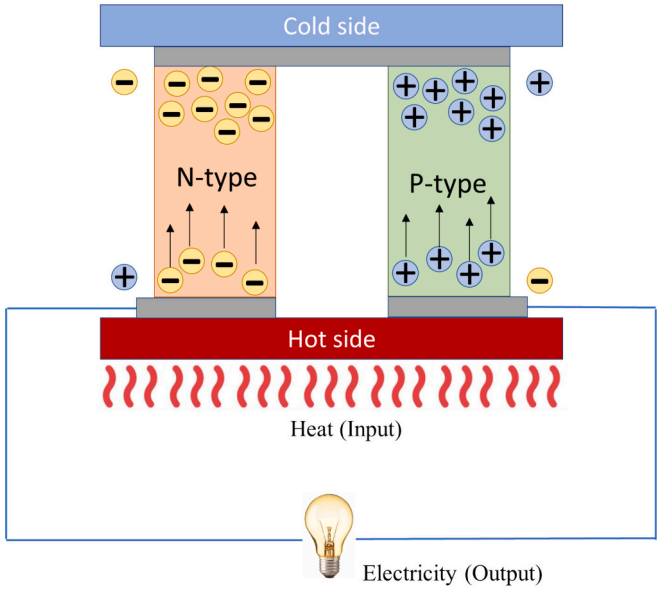

Fig. 1. Illustration of Seebeck effect (TEG working principle).

with the diffusion potential [42]. At the equilibrium, the induced thermoelectric voltage (ΔV) is proportional to the temperature difference (ΔT). The Seebeck effect can be expressed as shown in Eq. ((1) [40].

$$S_{ab} = S_a - S_b = \frac{\Delta V}{\Delta T} \tag{1}$$

Where S_a and S_b are the absolute Seebeck coefficients of the TE materials a and b, S_{ab} is the relative Seebeck coefficient. The ΔV in the above equation is equal to the open circuit voltage (V_{OC}) in a thermocouple that has a temperature gradient imposed. The Seebeck coefficient of a TE material is a temperature-dependent material property. Metals normally exhibit very low S while semiconductor materials, such as Silicon (Si), Germanium (Ge), and Selenium (Se), exhibit high S [43]. The p-type material has a positive Seebeck coefficient while the n-type material has a negative Seebeck coefficient.

TEC utilizes the Peltier effect as the working principle. The Peltier effect can be conceived as the opposite of the Seebeck effect. Simply, it states that when an electric current is passed through a junction connecting two TE materials, a temperature gradient is generated across the materials allowing them to either produce heat or cooling effect at the other junction (cold side) [43], as illustrated in Fig. 2. The generated thermal energy (i.e., heating or cooling) is proportional to the electric current and can be evaluated as shown in Eq. ((2) [12,40].

$$\dot{Q} = (\Pi_a - \Pi_b)I \tag{2}$$

Where Π_a *and* Π_b are Peltier coefficients of TE materials, $\dot{Q} = \frac{dQ}{dt}$ is heat power (also known as Peltier heat), I is electrical current.

The Peltier coefficient is not normally measured in research work as it can be obtained according to Eq. ((3) which describes the relationship between the Seebeck and Peltier coefficients.

$$\Pi = ST \tag{3}$$

The last thermoelectric effect is known as the Thomson effect (Fig. 3) which states that in the presence of both an electric current and a temperature gradient, thermal energy (either heating or cooling) is produced in a conductive material such as metals [7,40]. The generated thermal energy can be calculated according to Eq. ((4) [40,43].

$$q_x = \tau I \frac{dT}{dx} \tag{4}$$

Where τ is the Thomson coefficient, I is the electrical current, $\frac{dT}{dx}$ is the temperature gradient, and q_x is the generated thermal energy. The Thomson effect is responsible for the temperature dependence of the Seebeck coefficient. τ and S are related to each other according to Eq. ((5) [12].

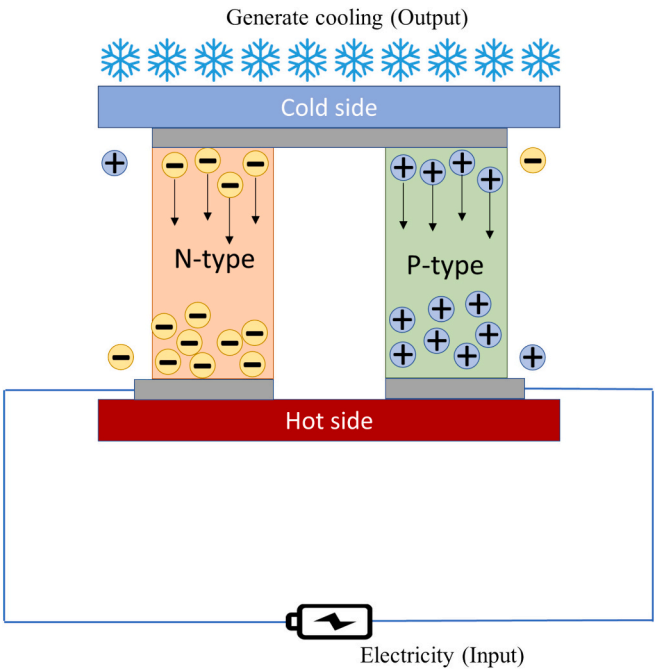

Fig. 2. Illustration of Peltier effect (TEC working principle).

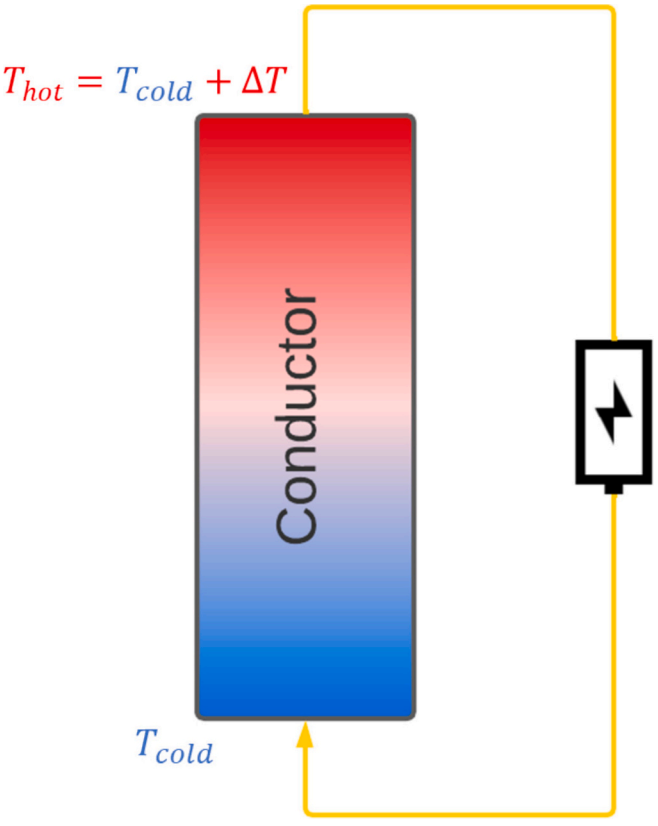

Fig. 3. Illustration of Thomson thermoelectric effect.

$$\tau = T\frac{dS}{dT} \tag{5}$$

Generally, the contribution of the Thomson effect to the energy conversion process in the TEMs is very limited and therefore it is normally neglected [40].

2.2. Thermoelectric properties

The performance of a thermoelectric material is estimated using a dimensionless value known as thermoelectric figure-of-merit (ZT) which can be computed according to Eq. ((6) [44].

$$ZT = \frac{S^2\sigma T}{\kappa} \tag{6}$$

Where σ is the electrical conductivity, S is the Seebeck coefficient, T is the absolute temperature, and κ is the thermal conductivity [45]. A high value of ZT indicates a good TE performance and a high conversion efficiency. Therefore, the effective TE material should have high electrical conductivity, low thermal conductivity, and high Seebeck coefficient [7,46]. However, maximizing ZT is challenging because κ, σ and S are interdependent [47]. For example, increasing the charge concentration increases the electrical and thermal conductivity but decreases the Seebeck coefficient [48]. Thus, it is important to optimize these three conflicting parameters in order to achieve the best possible ZT performance.

The power factor (PF), as given in Eq. ((7), is another important performance indicator of the TE materials because it evaluates the combined effects of σ and S [49].

$$PF = S^2\sigma \tag{7}$$

S and σ can be obtained based on Boltzmann transport theory which can be described according to Eqs. ((8) and ((9) [1].

$$S = \left(8\pi^2 {k_B}^2/3eh^2\right)m^* \times T \times \left(\frac{\pi}{3n}\right)^{2/3} \tag{8}$$

$$\sigma = ne\mu \tag{9}$$

Where $k_B = 1.380649 \times 10^{-23}\ J.K^{-1}$ is the Boltzmann constant, $e = 1.60217663 \times 10^{-19}\ C$ is the elementary charge, $h = 6.62607015 \times 10^{-34}\ J.HZ^{-1}$ is the Planck constant, m^* is carrier effective mass, n is the carrier concentration, μ is the carrier mobility. n and μ can be calculated using Eqs. ((10) and ((11) [50].

$$n = 1/(eR_H) \tag{10}$$

$$\mu = \sigma R_H \tag{11}$$

Where R_H is Hall coefficient [50].

κ is composed of two components including electronic thermal conductivity (κ_E) and lattice thermal conductivity (κ_L), as explained in Eq. ((12). κ_E expresses the holes and electrons transport heat while κ_L expresses phonons travelling through the lattice.

$$\kappa = \kappa_E + \kappa_L \tag{12}$$

κ_E can be estimated from σ using Wiedemann-Franz law as shown in Eq. ((13) [1].

$$\kappa_E = L\sigma T \tag{13}$$

where L is the Lorenz number which can be calculated using Boltzmann's constant as explained in Eq. ((14) [51,52].

$$L = \frac{\pi^2}{3}\left(\frac{k_B}{e}\right)^2 = 2.44 \times 10^{-8}\ V^2K^{-2} \tag{14}$$

Assessing the performance of TEM is normally achieved by calculating their energy conversion efficiency. Considering that the TEM is composed of multiple TE elements (i.e., thermocouples), it is vital first to calculate the figure-of-merit for a TE element. The figure-of-merit for a TE element, combining p- and n-type materials, can be defined according to Eq. ((15) [6,53,54].

$$ZT_{(NP)} = \frac{(S_P - S_N)^2 \times T}{\left(\left(\rho_N\kappa_N\right)^{0.5} + \left(\rho_P\kappa_P\right)^{0.5}\right)^2} \tag{15}$$

Where ρ_n and ρ_P are the electrical resistivity (note that $\rho = 1/\sigma$).

The maximum conversion efficiency of a TE element working in power generation mode, i.e., TEG, can be obtained based on $ZT_{(NP)}$ value and the temperature difference between the hot and cold sides as explained in Eq. ((17) [7].

$$\eta_{max(TEG)} = \frac{P_{elec}}{\dot{Q}_h} = \frac{T_{Hot} - T_{Cold}}{T_{Hot}} \times \frac{\sqrt{1 + ZT_{(NP)}} - 1}{\sqrt{1 + ZT_{(NP)}} + \frac{T_{Cold}}{T_{Hot}}} \tag{16}$$

Where P_{elec} is the produced electrical power, $\dot{Q}_h$ is the input heat flow at the hot side, T_{Cold} and T_{Hot} are the temperatures of the cold and hot reservoirs, respectively. It is worth noting that $\eta_{max(TEG)}$ forms a fraction of the ideal Carnot limit, or the maximum possible efficiency of a heat-based engine, given in Eq. ((17) [47].

$$\eta_{Carnot} = \frac{T_{Hot} - T_{Cold}}{T_{Hot}} \tag{17}$$

The performance of a TE element working in colling mode, i.e., TEC, is estimated by the Coefficient of Performance (COP). The maximum CoP can be computed as shown in Eq. ((18) [43,46].

$$CoP_{max(TEC)} = \frac{\dot{Q}_c}{P_{elec}} = \frac{T_{Cold}}{T_{Hot} - T_{Cold}} \times \frac{\sqrt{1 + ZT_{(NP)}} - \frac{T_{Hot}}{T_{Cold}}}{\sqrt{1 + ZT_{(NP)}} + 1} \tag{18}$$

Where P_{elec} is the supplied electrical power, $\dot{Q}_c$ is the generated cooling capacity (i.e., the rate of absorbed heat).

From Eqs. ((16) and ((17), it is clear that in order to improve the overall conversion efficiency of a TE device, the focus should be on optimizing the ZT value of the thermoelectric couple (Eq. ((15)) rather than the individual legs (Eq. ((6)). This can be achieved through selecting the p-type and n-type materials with peak ZT value at the average temperature of the device [55].

The $ZT_{(NP)}$, in Eqs. ((16) and ((17), is normally assessed at the mean temperature (T_m) of the hot and cold sides. T_m is given in Eq. ((19).

$$T_m = 0.5 \times (T_{Hot} + T_{Cold}) \tag{19}$$

2.3. Thermoelectric materials

TE materials can be either organic, inorganic, or hybrid. Such materials can further be divided according to the operating temperature into low-temperature materials operating at 273–500 K, medium-temperature materials operating at 500–900 K, and high-temperature materials operating at 900–1300 K [56].

The organic TE materials are conductive polymers such as poly (3, 4-ethylene dioxythiophene) (PEDOT) poly (styrene sulfonate) (PEDOT: PSS), polypyrrole (PPy), polyaniline (PANI), etc. On the positive side, these materials offer several advantages such as low cost, low thermal conductivity, low density, good mechanical flexibility, and low environmental impact [1,11,57]. However, on the negative side, these polymers are characterized by a low Seebeck coefficient and low electrical conductivity which in turn lower their overall TE performance [35]. Therefore, chemical and electrochemical doping techniques are normally used to improve the TE properties of these conductive polymers. With their low thermal conductivity and high mechanical compliance, organic TE materials are mainly suitable for making flexible and wearable TE devices for low-temperature heat recovery applications [58]. The TE polymers are synthesized using electrochemical polymerization and wet-chemistry polymerization techniques [59]. In practical applications, the organic TE materials can either be in thin-film or bulk

material forms. Solution-based techniques, such as inkjet and spin coating; and vacuum deposition techniques, such as thermal evaporation and sputtering, are commonly used to deposit thin films of various organic thermoelectric [60]. On the other side, high-pressure and high-temperature processing techniques, such as extrusion and hot-pressing, are utilized to prepare bulk organic TE conductive polymer [60].

The inorganic TE materials are semiconducting compounds such as BiTe-based materials, half-Heusler, skutterudites, and oxides. Such materials exhibit good TE performance represented by high power factor and figure-of-merit under a wide range of temperatures. On the other side, some of the inorganic TE materials have some disadvantages including scarcity, high cost, toxicity, and relatively poor processibility [11]. For the low-temperature range, BiTe, AgS, and SbTe are the most popular options. In particular, Bi_2Te_3-based TE materials, including n-type $Bi_2Te_{3-y}Se_y$ and p-type $Bi_xSb_{2-x}Te_3$, have attracted intense research due to its promising TE properties near room temperature [61,62]. Such materials can be applied in wearable thermoelectric modules to convert human body heat to power health monitoring sensors [48]. Another application for low-temperature TE materials is powering intelligent sensors (nodes) used in IoT (Internet of Things) field [47]. For the mid-temperature range, half-Heuslers, skutterudites. PbTe, and PbSe have received considerable research [63,64]. These materials are important for waste heat recovery applications of many industrial processes such as cement, steel, and metallurgy [65]. The high-temperature TE materials, such as CuSe, CuTe and oxides, can be utilized for waste heat recovery from different industrial equipment such as copper reverberatory furnace, zinc refining furnaces, aluminium refining furnaces, glass melting furnaces, etc. [1]. The inorganic TE materials are fabricated using different routes and by applying a combination of different processing techniques that can broadly be divided into two stages: a) preparing an alloy and b) sintering. The most popular fabrication route involves using a mechanical alloying approach, i.e., ball milling, to prepare TE alloy powder and then apply one of the sintering techniques, such as hot-pressing, pulse plasma sintering, and spark plasma sintering, to consolidate the powder into ingots or pellets. This route is suitable for TE materials with high melting temperature [40]. Another fabrication route involves using melting techniques, such as arc melting and melt spinning, instead of ball milling. In this approach, melting of the precursor elements takes place in an evacuated quartz tube followed by quenching using oil, water, or liquid nitrogen to form ingots. The obtained ingots are normally annealed to improve their mechanical properties and then grounded into powder to be used in the sintering process.

The hybrid TE materials are simply composites of organic conductive polymers with nanofillers. The nanofillers can be either inorganic TE nanoparticles or carbon nanofillers, such as carbon fibres, carbon nanotubes (CNTs), and graphite, due to their high electrical conductivity [11]. The TE properties of hybrid materials depend significantly on the shape and size of the nanofillers. The hybrid TE materials are typically fabricated by solution mixing in an organic solvent. The hybrid materials are broadly considered for low-temperature applications.

Table 1 and Table 2 summarize the advantages and disadvantages of different types of TE materials and possible waste heat recovery applications for each type.

Table 1
A summary of advantages and disadvantages of organic and inorganic TE material [35,49,124].

TE Materials Classification	Advantages	Disadvantages
Organic	Lightweight Environmentally friendly Cheap Low thermal conductivity High mechanical compliance so they are suitable for flexible TE devices.	Low Seebeck coefficient. Low electrical conductivity. Limited applications due to low TE performance.
Inorganic	High power factor. High figure-of-merit. Good performance under wide range of temperatures. Wide range of heat-recovery applications.	High cost of production per power output. Inflexibility and limited shape conformity. Heavy. Brittle. Health and safety risks due to toxicity of some semiconductor materials.

Table 2
Temperature range with typical TE materials and possible waste heat recovery applications [1,48].

Temperature range	Typical TE material family	Possible waste heat recovery applications
Low temperature (273–500 K)	Organic and hybird TE materials. BiTe BiSbTe AgSe SbTe	Sensors and devices for Internet of Things (IoT). Neurological implantable devices. Wearable personal health devices. Other medical diagnostic and rehabilitation applications.
Medium temperature (500–900 K)	Half-Heuslers Skutterudites PbTe PbSe GeTe AgSbTe SnSe SnTe	Drying And Baking Ovens (503–873 K). Steam Boiler Exhaust (503–753 K). Reciprocating Engine Exhaust (588–873 K). Gas Turbine Exhaust (643–813 K). Reciprocating Engine Exhaust (Turbo Charged) (503–643 K). Heat Treating Furnaces (698–923 K). Annealing Furnace Cooling System (698–923 K). Catalytic Crackers (698–923 K).
High temperature (900–1300 K)	CuSe CuTe LaTe CuS PrTe FeSi Oxides ($Ca_3Co_4O_9$, $CaMnO_3$, ZnO)	Aluminium Refining Furnace (923–1033 K). Zinc Refining Furnace (1033–1373 K). Steel Heating Furnace (1198–1323 K). Copper Refining Furnace (1033–1088 K). Copper Reverberatory Furnace (1173–1373 K). Open Hearth Furnace (923–973 K). Hydrogen Plants (923–1273 K). Cement Kiln (Dry Process) (893–1003 K). Solid Waste Incinerators (923–1273 K). Fume Incinerators (923–1723 K).

3. Additive manufacturing of thermoelectric materials and modules

Unlike subtractive manufacturing technologies (turning, milling, laser cutting, etc.) that involve material removal, AM refers to a process of building a part by adding the material layer upon layer. ISO/ASTM 52900:2015 standard specifies seven main categories of AM namely Photopolymerization (VP), Material Jetting (MJ), Binder Jetting (BJ), Material Extrusion (ME), Directed Energy Deposition (DED), Sheet Lamination (SL), and Powder Bed Fusion (PBF) [66,67].

Regardless of the AM category, the AM process workflow, as illustrated in Fig. 4, is divided into three phases, including pre-processing, processing, and post-processing transferring, a digital CAD model into a physical part. The pre-processing phase involves four steps. In the first step, a 3D CAD model that fully describes the geometry of the

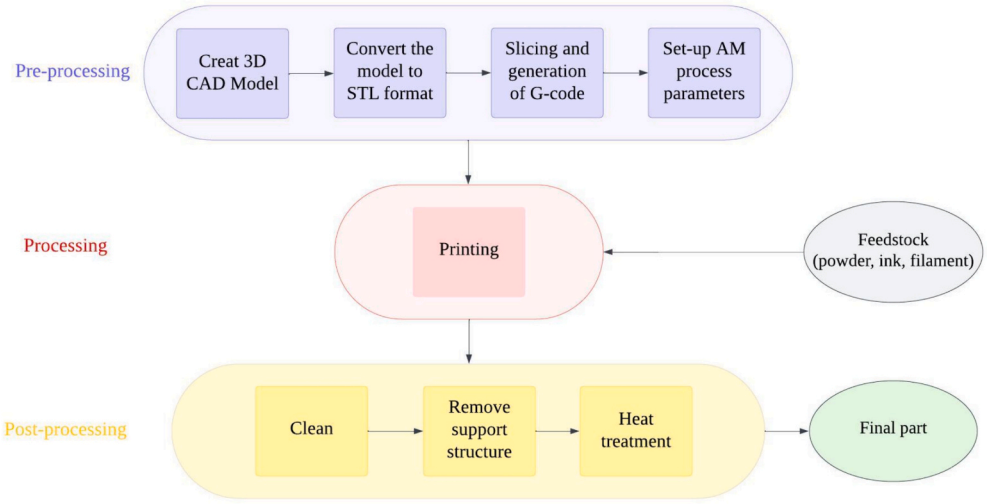

Fig. 4. AM process workflow.

part is established. The second step involves converting the CAD model into STL (Standard Tesselation Language) file format as it is the standard format recognised by all AM systems; and contains only the surface geometry data of a 3D CAD model. In the third step, the STL file is transferred to a slicing software, which can be part of the AM system, to divide the model into a specific number of layers and generate G-Code to control the components of the AM system during the building process. The last step of the pre-processing phase is to prepare the AM machine by setting up the build parameters such as speed, atmosphere, temperature, etc. The processing phase involves the actual building process which is conducted automatically by the AM system with minimal human monitoring or supervising. Once the building is completed, the post-processing phase starts where the part undergoes some necessary treatments, such as removing the additional support structures, cleaning, and heat treatment, before it is ready to be used.

This section will explore the different AM technologies that were recently adopted for manufacturing TE materials and modules. The section is limited to PBF, MJ, and ME technologies as they are the main AM methods used for fabricating TE materials.

3.1. Powder bed fusion (PBF)

3.1.1. Overview of PBF

PBF takes its name from using powder as a starting material which is placed on a platform, known as a powder bed, and then processed by irradiating their particles, to fuse them together, using a thermal energy source. Depending on the type of the thermal energy source, there are three main types of PBF including Selective Laser Melting (SLM), Selective Laser Sintering (SLS), Electron Beam Melting (EBM). A laser beam is used in SLM and SLS to melt and sinter the powder particles, respectively. For EMB, an electron beam is utilized as a heat source to melt the powders.

SLM is the most used PBF technique for additive manufacturing of TE material. In this process, a thin layer of the powder is first deposited in the powder bed. Then, a highly focused laser beam, with power (~100–1000 W) and small spot size (~20–100 μm), selectively scans the powder bed at high speed (~0.05–4 $m.s^{-1}$) melting the powder particles line by line and creating a melt pool. The molten material then rapidly solidifies and bonds with the adjacent material creating a solid layer of the part. To inhibit oxidation and reduce oxygen pickup by the molten material, an inert environment, such as nitrogen, argon, and helium, is normally used to protect the molten pool during the SLM process.

There are different factors that influence the SLM process and the quality of the printed part. These factors include the powder characteristics, such as particle shape and size, laser parameters such as laser power (P_{laser}), hatch distance (h), laser beam diameter (D), and scanning velocity (v) $\left[m.s^{-1}\right]$, and build parameters such as layer thickness (t) and build orientation. Among the aforementioned factors, P, h, t, and v are the most important as they determine the Energy Density (ED) irradiated by the laser beam on the powder bed. ED can be determined at different dimensions including linear (E_L), areal (E_A), or volumetric (E_v) which can be computed according to Eqs. ((20), ((22), ((21), respectively [68].

$$E_L = \frac{P_{laser}}{v} \tag{20}$$

$$E_A = \frac{P_{laser}}{v \times h} \tag{21}$$

$$E_v = \frac{P_{laser}}{v \times h \times t} \tag{22}$$

P, h, t, and v should be optimized to ensure that an adequate amount of ED is provided to the powder bed as inadequate ED may degrade the quality of the as-printed part. For example, high ED may vaporise the powder particles, instead of only melting them, generating bubbles in the melt pool, which may get trapped during the solidification phase forming gas pores within the fabricated part [69]. On the other side, low ED may be insufficient to melt all the powder particles leaving some unmelted particles which in turn cause defects known as incomplete fusion holes [70].

SLM (Fig. 5) is a complex process as a series of physical and chemical interactions, such as laser energy absorption, different heat modes, laser scattering, spattering, etc., take place in the molten pool once the laser beam impinges the powder bed. Due to such complex interactions, the as-printed parts may contain different types of defects such as residual stresses, micro-cracks, pores, voids, inclusions, un-melted powder, high surface roughness, etc. [71,72]. Therefore, post-printing treatments, such as annealing, electropolishing, hot isostatic pressing, and ultrasonic impact treatment, are normally conducted to reduce the negative consequences of these defects and to improve the mechanical and functional performance of the parts [73].

3.1.2. PBF of TE materials

The laser beam was used as a heat source for melting and sintering different types of TE powder such as β-$FeSi_2$ [74], oxides [75], Bi_2Te_3 [76], SnTe [77], skutterudite-based materials [14], etc. Among the earlier studies, Kinemuchi et al. [75] demonstrated the feasibility of laser melting technique to synthesize various types of TE compounds including binary systems (Bi—Sb and Mn—Se), ternary system (Mn-Al-

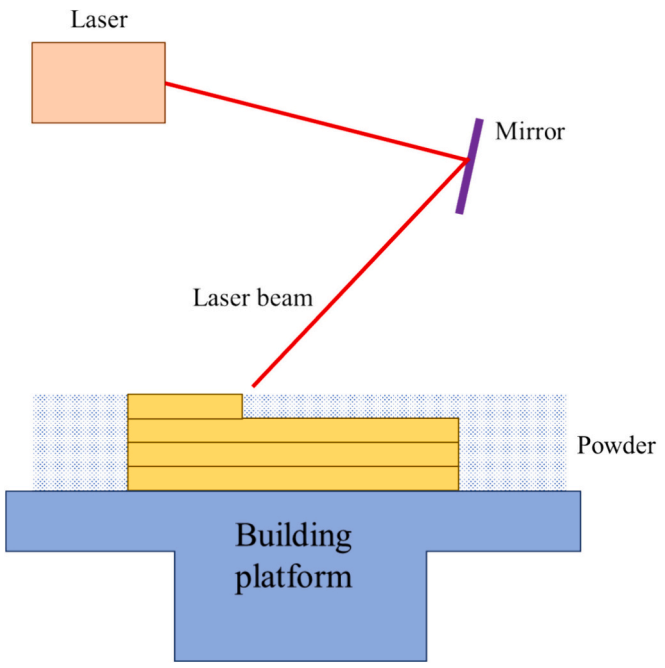

Fig. 5. Schematic of SLM process.

Si), and oxides ($Ca_3Co_4O_9$ and $SrTiO_3$). The laser was used to irradiate a single powder layer of each material. Helium (He) environment was used in the processing chamber for binary and ternary alloys while ambient air was used for oxides. It was found that the compositional differences between the laser-treated material and the starting material are minimal and negligible proving the ability of laser to fabricate such materials.

As one of the best room-temperature TE materials, Bi_2Te_3 was the most studied material for SLM fabrication. El-Desouky et al. [76] were among the first researchers who used SLM to fabricate Bi_2Te_3 TE materials. As the Bi_2Te_3 powder has insufficient flowability and spreadability, it was first compacted, using a hydraulic press, into disks with a thickness of $\sim 0.5\,mm$ and then single melt lines were formed on the surface of these disks. The effects of laser processing parameters on the densification and microstructure of the melt lines are investigated. Completely consolidated particles were observed at the centre of the scan line while partially consolidated particles were formed at the edges. Increasing the laser power resulted in increasing the width of the fully melted region. Powder consolidation beneath the melt line was observed for disks processed with 5 W laser power indicating the ability of the laser beam to generate sufficient melting depth and process at least one complete layer of powder. The surface of the processed disks contained randomly oriented microcracks which are common defects in Selectively Laser Melted (SLMed) materials. Such findings provided evidence that SLM can be used to process Bi_2Te_3. In another work, El-Desouky et al. [39] studied the influence of the laser energy density on the consolidation of Bi_2Te_3 powder and the microstructure of SLMed material. It was found that the porosity of the processed material decreases by increasing the power density, as shown in Fig. 6. The power density not only affected the porosity content within the processed material but also affected the shape and size of the pores. Spherical-shaped pores were mainly observed within the molten region while pores with irregular shapes were formed at the interface between the molten region and the powder compact. The high-power density of the laser enabled a complete melting of the specimen while the low-power density only melted the specimens partially.

Carter et al. [78] used a nanosecond pulsed laser to selectively melt Bi_2Te_3 powder compacts. It was found that laser power in the range of 3 W to 5 W can generate significant subsurface melting and consolidation up to a depth of 20–100 μm. The microstructure of the SLMed material

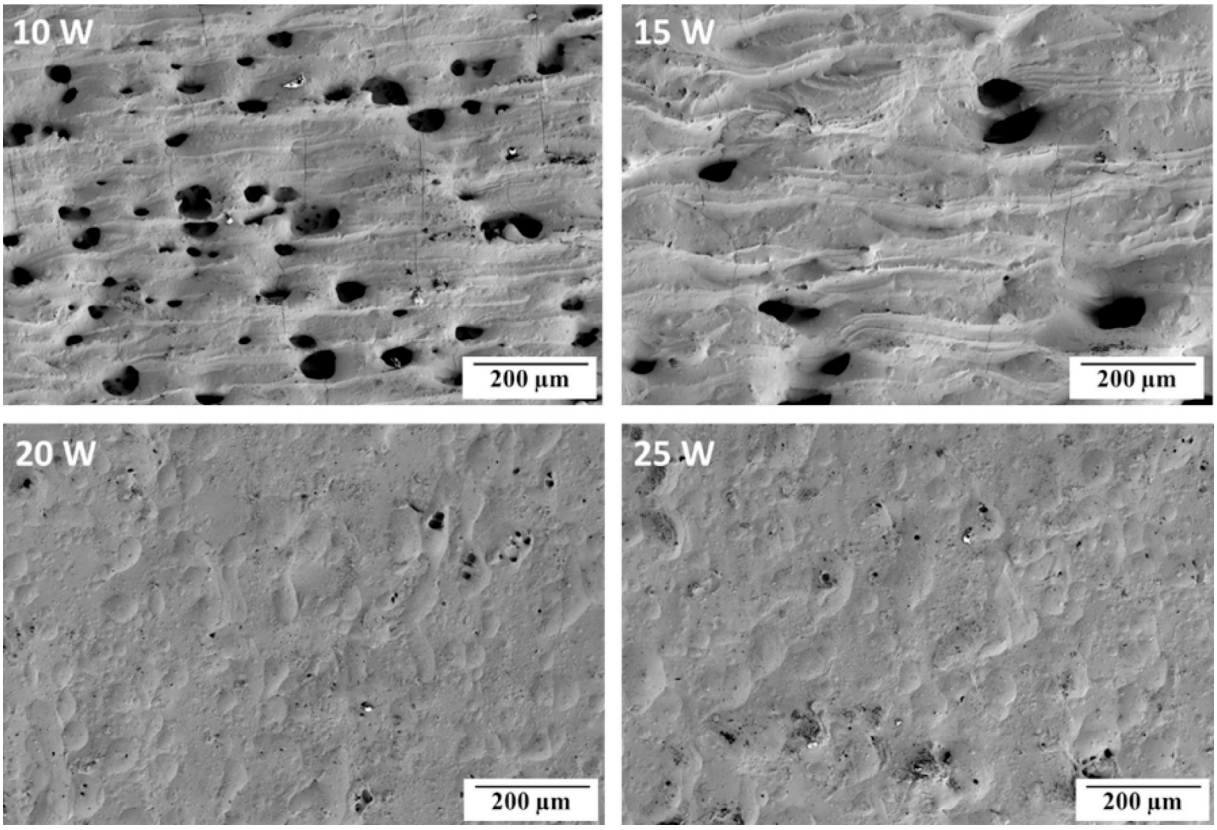

Fig. 6. SEM micrographs showing the influence of power density on the porosity of SLMed Bi_2Te_3 [39].

was composed of fine columnar grains. The fabricated material exhibited some defects such as microcracking and high surface roughness. The authors indicated that applying thermal management for the powder bed, i.e., controlling the temperature of the substrate, may allow SLM of TE material with a smaller number of defects. Zhang et al. [79] were the first who applied SLM on loose Bi_2Te_3 powders. The SLM process was conducted in an inert environment of nitrogen (N_2) where the level of oxygen was maintained below 4%. The laser power, hatch distance, and scan speed were set to 25W, 37.5 μm, and 500 mm.s^{-1}, respectively, resulting in an overall laser energy density of 1.3 J.mm^{-2}. The process proved to be successful as the printed material exhibited 88% relative density and good consolidation within and between the layers. The SLM process did not alter the structure of the Bi_2Te_3 as the XRD spectrum of the SLMed materials matched well the one of Bi_2Te_3 powders. The authors also characterized the thermoelectric, thermal, and electrical properties, including Seebeck coefficient, thermoelectric figure-of-merit, electrical conductivity, thermal diffusivity, specific heat, and thermal diffusivity, of the SLMed samples at room and elevated temperatures. The room-temperature properties varied from sample to sample where the values of Seebeck coefficient and electrical resistivity were in the ranges of 85–189 μV·K^{-1} and 1–15 mΩ.cm, respectively. All the measured properties were temperature-dependant, as shown in Fig. 7, due to the evolution of crystalline point defects, carriers, and mobility with temperature. The best ZT value of 0.11 was obtained at temperature of 50°C.

Zhang et al. [80] identified the SLM process parameters to fabricate Bi_2Te_3. The used Bi_2Te_3 powder in this work had particles with irregular shapes (non-spherical) and sizes of <53 μm. The angle of repose for Bi_2Te_3 powder was ~ 50.67° indicating a poor flowability of this powder compared to the other metallic or ceramic materials used in SLM. Inert gas (nitrogen or argon) was used in the building chamber to maintain a low oxygen level of <4% during the SLM process. It was reported that the disks manufactured with volumetric energy density in the range of 9 to 11 J.mm^{-3} had sufficient relative density and good mechanical strength to resist fracture during handling. The study suggested that the optimal SLM parameters are a laser power of 25W, a scan speed of 500 mm.s^{-1}, a hatch distance of 37.5 μm, and a powder layer thickness of 150 μm.

In addition to the standard Bi_2Te_3 material, SLM was also applied to form its n-type version $Bi_2Te_{2.7}Se_{0.3}$. Mao et al. [81] used SLM for fabricating bulk n-type $Bi_2Te_{2.7}Se_{0.3}$ TE material. Self-propagating High-temperature Synthesis (SHS) was first used to produce $Bi_2Te_{2.7}Se_{y0.3}$ ingots and then these ingots were grinded to obtain the powder. The SLM build substrate was formed by using Spark Plasma Sintering (SPS) for some of the $Bi_2Te_{2.7}Se_{0.3}$ powder. To facilitate easy spreading, a slurry with a solid content of 17 vol% was prepared by mixing the $Bi_2Te_{2.7}Se_{0.3}$ powder with alcohol. The results of the study revealed that in order to produce a high forming quality of this material, the laser energy density should be controlled between 10 and 33.3 J.mm^{-3} while the laser power should be <8 W. It was found that the chemical composition of the fabricated materials is sensitive to the laser energy densities as the densities >33.3 J.mm^{-3} caused evaporation of Se and Te. The SLMed materials yielded ZT value of 0.84 at 400 K which is comparable to that of the commercial material.

Wu et al. [82] combined non-contact dispenser printing with SLM to fabricate n-type $Bi_2Te_{2.7}Se_{0.3}$ material. Ball mill dispersion is used to prepare $Bi_2Te_{2.7}Se_{0.3}$ slurry from $Bi_2Te_{2.7}Se_{0.3}$ powder mixed with small amounts of additives (Tween 20 and antitoam AR) which helped to achieve suitable rheological properties of the slurry. The slurry is then placed in a nozzle dispenser which is used to prepare a smooth powder layer for the SLM process. Successful SLM printing was achieved with a laser power density of 16.7 J.mm^{-3} which yielded high-quality layers with only limited vaporization of Te and Se and without any balling. Following the SLM, the printed material was annealed at 673 K for 36 h to restore its homogeneity. The formed bulk $Bi_2Te_{2.7}Se_{0.3}$ material exhibited thermoelectric properties comparable to those materials prepared by conventional methods such as Zone Melting (ZM) and SHS as shown in Fig. 8.

Welch et al. [83] studied the nano- and micro-structures of SLMed $Bi_2Te_{2.7}Se_{y0.3}$. $Bi_2Te_{2.7}Se_{y0.3}$ ingots were ball milled and sieved to generate the $Bi_2Te_{2.7}Se_{y0.3}$ powder with a nominal effective diameter of <75 μm. The obtained powders were placed manually on the powder bed and flattened using a stainless steel roller. The building was completed in an argon environment using SLM process parameters of 25 W laser power, 37.5 μm hatch spacing, and 150 μm layer thickness. The measured relative density of the SLMed materials was 74%. The XRD results of the SLMed materials matched those of the raw powder indicating that the SLM process didn't generate any new phases. The grains of the SLMed material were columnar grains oriented in the build

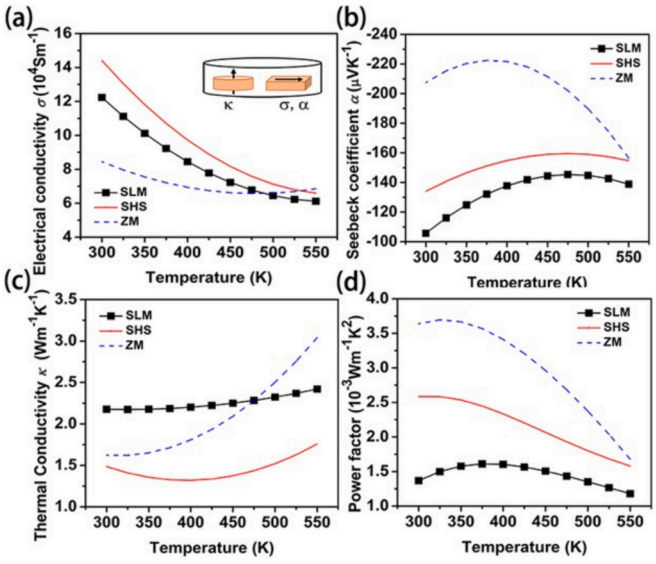

Fig. 8. Thermoelectric properties of SLMed and traditionally fabricated $Bi_2Te_{2.7}Se_{y0.3}$ material [82].

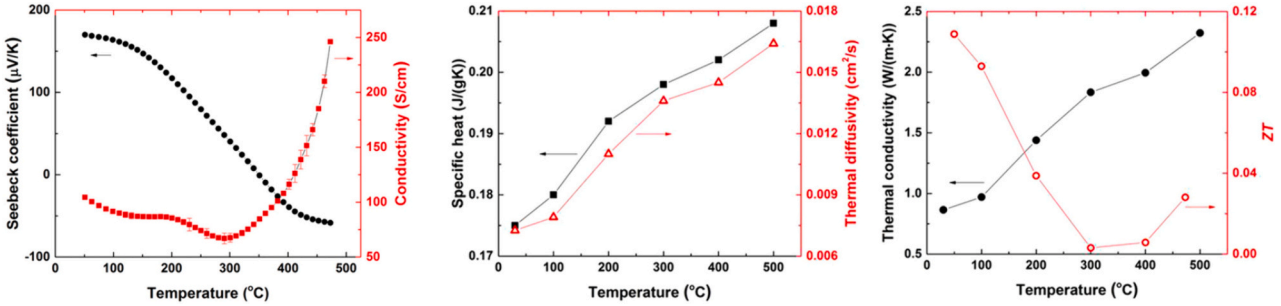

Fig. 7. The temperature-dependant thermal, electrical, and thermoelectric properties for the SLMed Bi_2Te_3 [79].

direction and spanned through several layers. The SLMed material contained multi-scale pores, microscale cracks, low-angle grain boundaries, and nanoscale inclusions. The pores had spherical and aspherical shapes, as can be seen in Fig. 9, and they are caused by the keyhole processing mode and lack of powder fusion. The microscale cracks (Fig. 9) are caused by the residual stresses resulted due to the temperature gradients in the melt pool. The nanoscale oxide inclusions appeared at different locations, and they were different in size (aspect ratio) and composition. It was found that the fabricated material had a maximum Seebeck coefficient of 143 $\mu V{\cdot}K^{-1}$ at 95 °C. This positive Seebeck coefficient indicates that SLM process shifted the material from n-type material to p-type material. Such shift is due to oxide inclusions which change the primary charge carriers of the material from electrons to holes.

Xiong et al. [84] used SLS to prepare TE materials from a composite powder of E12 epoxy resin binder and n-type $Bi_2Te_{2.85}Se_{y0.15}$ with a weight ratio of 1:7. The homogeneous composite powder was obtained using mechanical mixing (ball milling) for 2 h. Degreasing treatment was used to remove the E12 binder after the SLS process. The influence of SLS process parameters on the relative density of the TE material was explored and found that the laser power has the most impact while the scanning speed has the lowest effect. The prepared TE material exhibited a maximum ZT of 0.88 at 350 K when fabricated using a laser power of 20 W, a scanning interval of 0.26 mm, and a scanning speed of 3000 mm. s^{-1}.

SLM was also used as a forming process for p-type Bi_2Te_3-based materials ($Bi_xSb_{2-x}Te_3$). Shi et al. [85] studied the thermoelectric performance of a 3D-printed porous $Bi_{0.5}Sb_{1.5}Te_3$ material in the temperature range of $25^{\circ}C - 250^{\circ}C$. Ball milling was used to prepare the feedstock powder. The porous structure was achieved by adjusting the printing parameters as such they only partially melt the powder particles. The motivation for fabricating porous TE material was to reduce the thermal conductivity while maintain the electrical conductivity, thereby improving the overall figure of merit. The sizes of the pores and their distribution pattern were the main factors influencing the TE properties of the material. The microstructure characterization revealed that the Selectively Laser Sintered (SLSed) material had micro and nano-scaled pores. The thermoelectric performance analysis, as presented in Fig. 10, showed that the power factor, electrical and thermal

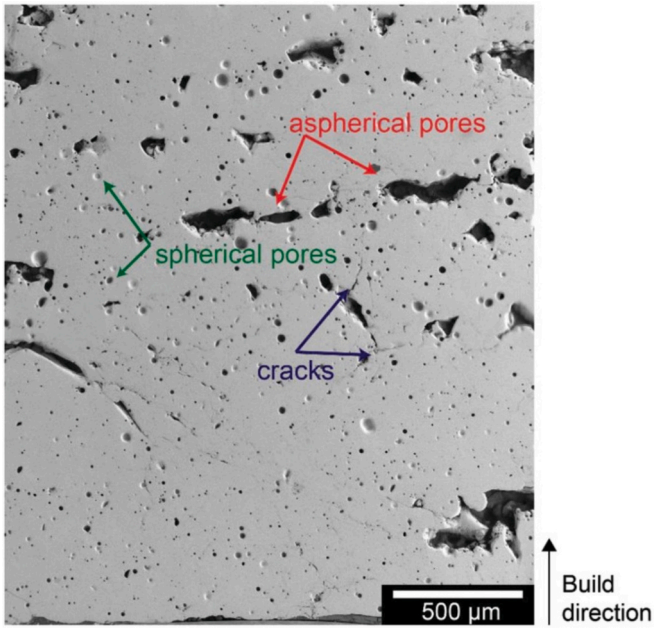

Fig. 9. SEM micrograph of SLMed $Bi_2Te_{2.7}Se_{y0.3}$ showing the pores and cracks [83].

conductivities of the 3D-printed porous material are less than those of the bulk material. On the other side, the porous material yielded a Seebeck coefficient and ZT higher than the bulk counterpart. The highest ZT value of the porous SLSed $Bi_{0.5}Sb_{1.5}Te_3$ material was 1.29.

Qiu et al. [50] fabricated p-type $Bi_{0.4}Sb_{1.6}Te_3$ TE material using SLM. Thermal explosion reaction was first used to prepare $Bi_{0.4}Sb_{1.6}Te_3$ ingot from cold-pressed pellet then ball milling was applied to produce $Bi_{0.4}Sb_{1.6}Te_3$ powder. The obtained powder was mixed with alcohol to generate a slurry that can be used in the SLM system. The SLM building was conducted in a protective environment of argon and hydrogen (Ar: H_2) with a volume ratio of 95:5. The thermoelectric and mechanical performance of the Additively Manufactured (AMed) material were compared to those prepared by traditional methods including ZM and SPS. The SLMed material showed anisotropic TE properties where its ZT value in the SLM building direction was 65% greater than that measured perpendicular to the building direction. The peak ZT value of the SLMed material in the building direct was 1.1 at 316 K which was slightly higher than the ZM-prepared material. The compressive strength of the SLMed material along the building direction was also greater than counterparts fabricated by ZM or SPS methods.

In addition to Bi_2Te_3-based material, Sb_2Te_3 is another low-temperature material which was fabricated by SLM. Shi et al. [38] determined the optimal SLM process parameter to fabricate p-type Sb_2Te_3 TE material. Ball milling was utilized to mix the Sb and Te powder together and then the powder mixture was used for the SLM process which is conducted in an argon atmosphere. The study revealed that the SLMed TE samples fabricated by low laser energy density have better TE properties compared to those fabricated by high energy density. The TE properties of the best SLMed sample, which is fabricated using laser energy density of 3 $J.mm^{-2}$, are Seebeck coefficient of 73 $\mu V{\cdot}K^{-1}$ electrical conductivity of 3.52×10^5 $S.m^{-1}$ and power factor of 19 $\mu W.cm^{-1}{\cdot}K^2$ at room temperature. The power factor of the SLMed material was greater than its zone-melted counterpart. The material offered a maximum ZT value of 0.4 at $250^{\circ}C$.

Besides its uses for low-temperature TE materials, many studies explored the feasibility of SLM for fabricating medium- and high-temperature TE materials. Yan et al. [65] formed n-type $CoSb_{2.8}Te_{0.15}$ skutterudite thermoelectric material using SLM. $CoSb_{2.8}Te_{0.15}$ powder was obtained by crushing an ingot obtained via a SHS technique. The powder was dispersed in ethanol to obtain a slurry with a solid content of 30 vol%. Argon was used as an inert gas while titanium substrate was used as the building platform. It was found that a laser power density in the range of 58–130 $J.mm^{-3}$ was able to produce high-quality layers of $CoSb_{2.85}Te_{0.15}$ material with flat and dense surfaces. As-built and annealed (at $450^{\circ}C$ for 4 h) SLMed samples were analysed. The microstructure of the as-prepared SLMed samples is composed of fine grains with $CoSb_2$, Sb, and $CoSb_3$ as main phases. For the annealed materials, its microstructure contained a few microcracks and composed of $CoSb_3$ as the main phase. It was reported that the fabricated SLMed bulk material contained submicrometer grain size and yielded a maximum ZT value of 0.56 at 823 K. The annealed material provided better thermoelectric performance than the as-built material, but lower performance compared to the SPS-fabricated material, as can be seen in Fig. 11.

Chen et al. [86] combined SLM with SPS for rapid fabrication of n-type and p-type filled skutterudites TE materials including $Yb_{0.4}Co_4Sb_{12.1}$, $In_{0.5}Co_4Sb_{12.1}$, and $Ce_{0.95}Fe_3CoSb_{12.1}$. The SLM with its fast melting and solidification rates reduced the peritectic segregation of Co—Sb precursor phases and confined them into zones with micro size. The SPS process is used in place of annealing to shorten the fabrication time from 9 days to <1 h. The SLM-SPS fabricated filled skutterudites exhibited very good ZT measurements of ~1.09 at 700 K for n-type $In_{0.5}Co_4Sb_{12.1}$, ~1.23 at 850 K for n-type $Yb_{0.4}Co_4Sb_{12.1}$, and ~ 0.79 at 750 K for p-type $Ce_{0.95}Fe_3CoSb_{12.1}$.

Chen et al. [77] analysed the influence of SLM process parameters on the quality and thermoelectric performance of p-type SnTe TE material. The powder for the SLM process was obtained by ball-milling of SHS-

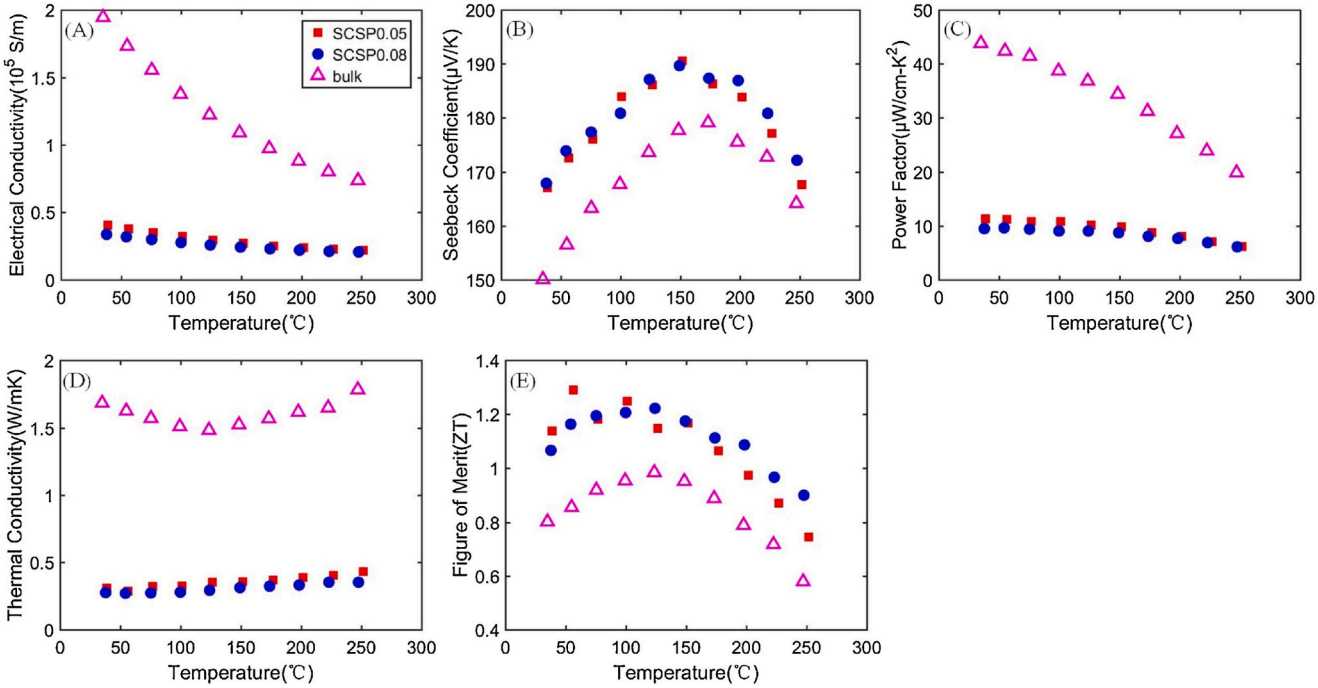

Fig. 10. Comparison of thermoelectric properties of SLSed porous and bulk $Bi_{0.5}Sb_{1.5}Te_3$ [85].

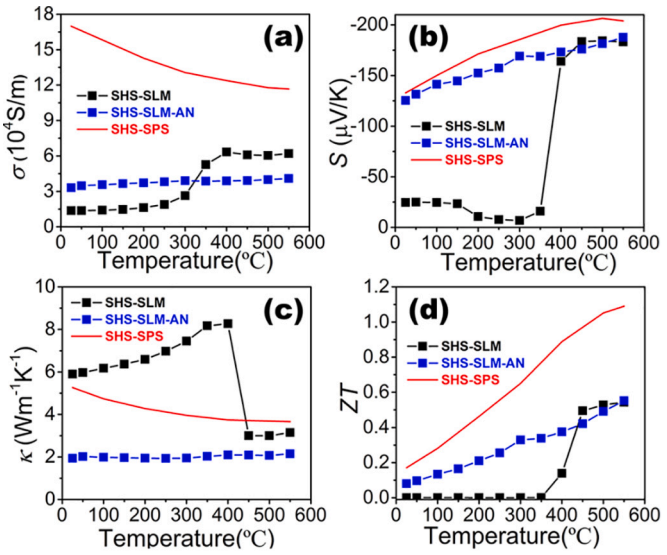

Fig. 11. Thermoelectric properties of SLMed, annealed SLMed, and SPS-prepared $CoSb_{2.8}Te_{0.15}$ skutterudite [65].

prepared SnTe ingot. The obtained non-spherical SnTe powder was mixed with alcohol to form a slurry, with 29 vol% alcohol, which was then deposited on SPS-formed SnTe substrate for the laser melting process. Argon atmosphere was used in the SLM process to minimize oxidation. The optimal SLM process parameter window was determined, and it was found that a laser with energy density in the range of 0.015–0.030 J.mm^{-1} can produce a good quality layer with a thickness of 25 μm. The SLMed material exhibited uniform chemical composition and contained nanograins with a size of 20–50 nm. Such nanostructure can reduce the thermal conductivity and improve the overall TE properties of the material. The SLMed material exhibited comparable thermoelectric performance to its traditionally-manufactured counterpart where the Seebeck coefficients of the SLMed and SPS materials were 28.08 and 29.77 μV·K^{-1}, respectively.

Zhang et al. [87] fabricated half-Heusler thermoelectric materials including half-Heusler ZrNiSn and $Hf_{0.3}Zr_{0.7}CoSn_{0.3}Sb_{0.7}$/nano-$ZrO_2$ using SLM. The SLMed materials were found to be porous with high surface roughness. The chemical compositions of the SLMed materials were slightly different compared to the starting compositions due to the oxidation and decomposition events associated with the SLM process. Yan et al. [88] investigated the possibility of combining SHS and SLM for forming half-Heusler ZrNiSn TE material. SHS was used to synthesize ingots which were subsequently crushed into powders to be processed using SLM. To facilitate the deposition of the powder in the SLM system, a slurry was prepared by mixing the ZrNiSn powder with anhydrous alcohol in a mass-to-volume ratio of 3:1 g.ml^{-1}. The SLM process was conducted using a titanium building platform and an inert environment of argon mixed with 10% hydrogen. It was found that a laser power density between 88 and 146 J.mm^{-3} can form a single layer of ZrNiSn with good surface quality. The SLM process led to the formation of a small amount of Sn phase which in turn increased the carrier concentration in the SLMed material. The SLMed material underperformed the material fabricated by a combination of SHS and SPS. The maximum ZT value of the SLMed ZrNiSn material was 0.39 at 873 K, as can be seen in Fig. 12.

Thimont et al. [89] studied the influence of laser power density and scanning speed on the microstructural and structural properties of SLMed Higher Manganese Silicide (HMS) sheet samples. Manganese and silicon powders were ball-milled; and then used in the SLM process which is conducted in an inert environment of argon. The material fabricated with moderate laser power of 91 J.cm^{-2} exhibited melted grains with good intergranular boundaries and good surface homogeneity. The XRD results of this material showed $MnSi_y$ phase which proved the capability of the laser to initiate the reaction between the manganese and the silicon. On the other side, the materials prepared with higher power density contained overmelted balls grains which normally yield brittle mechanical performance.

3.1.3. *Challenges and prospects of PBF for TE materials*

SLM is mostly used for metallic alloys, such as stainless steel [90], aluminium [91], titanium [92], *cobalt-chromium [93]*, silver [94], and copper [95], and it is rarely used for thermoelectric and other functional

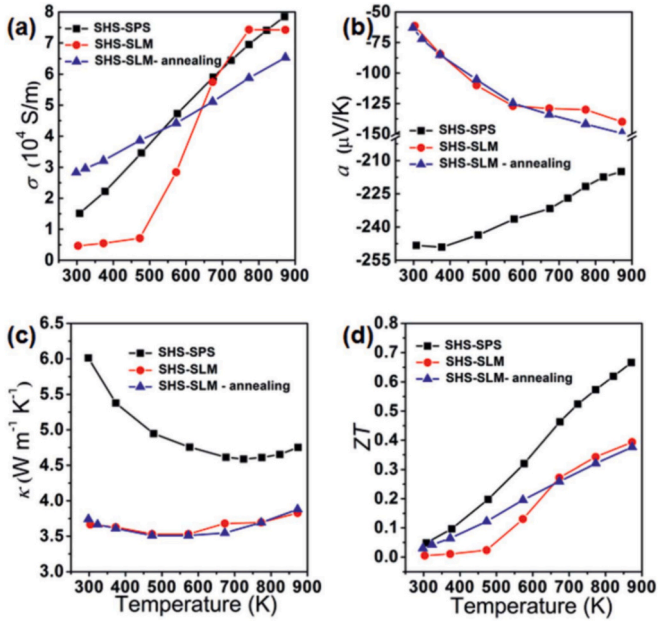

Fig. 12. Thermoelectric properties of SLMed, annealed SLMed, and SHS-SPS prepared ZrNiSn [88].

materials. Compared to metals, thermoelectric materials are characterized by lower thermal conductivity, lower boiling and melting points, weaker thermal shock resistance, and lower mechanical strength [96]. Therefore, it is more challenging to prepare thermoelectric materials using SLM. However, it is evident from the reviewed studies in Section 3.1.2 that the SLM process can successfully be used to fabricate various semiconductor materials with satisfactory thermoelectric performance for both low-temperature and high-temperature thermal-electric conversion. Table 3 summarizes the SLM process parameters and thermoelectric performance for some of the SLMed TE materials. It is clear from the data reported in this table that the SLMed materials subjected to post-SLM annealing treatment outperform the as-printed materials in terms of ZT measurements. Generally, annealing treatment improves the homogeneity of the material composition and enhances the uniformity of the TE properties resulting in better overall TE performance.

Among the specific advantages of SLM for TE applications is its ability to create nanostructured materials. Nanostructuring is one of the strategies to improve thermoelectric performance; and it means creating nanograins and introducing nano-scaled lattice defects, such as precipitates, dislocations and interfaces, etc. [1,97]. Nanostructuring assists in phonon scattering and reduces the lattice thermal conductivity of the material, thereby increasing ZT and improving the overall TE performance. SLM, with its high heating and cooling rate, can generate grains with nanoscale, as reported by Chen et al. [77], therefore PBF can be considered as a feasible nano-structuring approach of TE materials.

Despite its capability to fabricate TE materials with complex

Table 3
Summary of SLMed TE materials with SLM process parameters and TE properties.

Material	Type	Reported SLM process parameters	Post-processing	ZT_{max}	Reference
Bi_2Te_3	p-type	P = 25 W v = 500 mm.s^{-1} h = 0.0375 mm EA = 1.3 J.mm^{-2}	None	ZT = 0.11 at 323 K	[79]
$Bi_2Te_{2.7}Se_{0.3}$	n-type	Ev = 10–33.3 J.mm^{-3}	Annealing Temp = 673 K Time = 36 h	ZT = 0.84 at 400 K	[81]
$Bi_2Te_{2.7}Se_{0.3}$	n-type	E_V = 16.7 J.mm^{-3}	Annealing Temp = 673 K Time = 36 h	ZT = 0.3 at 450 K	[82]
$Bi_2Te_{2.85}Se_{0.15}$	n-type	P = 20 W v = 3000 mm.s^{-1} h = 0.26 mm	Degreasing treatment	ZT = 0.88 at 350 K	[84]
Porous $Bi_{0.5}Sb_{1.5}Te_3$	p-type	P = 30 W v = 3200 mm.s^{-1} h = 0.05–0.08 mm	None	ZT = 1.29 at 232 K	[85]
$Bi_{0.4}Sb_{1.6}Te_3$	p-type	–	None	ZT = 0.72 at 415 K (measured parallel to the building direction) ZT = 0.21 at 420 K (measured perpendicular to the building direction)	
			Annealing Temp = 673 K Time = 24 h	ZT = 1.1 at 316 K	[50]
Sb_2Te_3	p-type	P = 60 W v = 200 mm.s^{-1} h = 0.05 mm, Ev = 4.77 J.mm^{-3} EA = 3 J.mm^{-2}	None	ZT = 0.4 at 523 K	[38]
$CoSb_{2.8}Te_{0.15}$ skutterudite	n-type	Optimal processing window P = 12–16 W Ev = 56–130 J.mm^{-3}	Annealing Temp = 450C Time = 4 h	ZT = 0.56 at 823 K	[65]
$Yb_{0.4}Co_4Sb_{12.1}$ skutterudite	n-type	P = 150 W v = 200 mm.min^{-1} h = 3.75 mm t = 2 mm	SPS	ZT = 1.23 at 850	[86]
$In_{0.5}Co_4Sb_{12.1}$ skutterudite	n-type	P = 150 W v = 200 mm.min^{-1} h = 3.75 mm t = 2 mm	SPS	ZT = 1.09 at 700 K	[86]
$Ce_{0.95}Fe_3CoSb_{12.1}$ skutterudite	p-type	P = 150 W v = 200 mm.min^{-1} h = 3.75 mm t = 2 mm	SPS	ZT = 0.79 at 750 K	[86]
half-Heusler ZrNiSn	n-type	Optimal processing window Ev = 88–146 J.mm^{-3}	Annealing	ZT = 0.39 at 873 K	[88]

geometrical architecture, SLM still encompasses some technical and economic challenges. The economic challenge is associated with the high initial investment required due to the high cost of SLM systems. Also, it is challenging to use SLM to manufacture a full TEM continuously as the traditional SLM can only process one type of powder in a single build. Furthermore, the limited flowability of the commercial TE materials powder is another main challenge for processing them using commercial SLM systems. As it is known, the characteristics of powders, as starting material, play a key role in the SLM process and also influence the performance of the printed parts. Currently, commercial TE powders are prepared via mechanical comminution methods which produce particles with aspherical, flaky, and high aspect ratio shapes. Such shape characteristics are undesirable for SLM as they result in insufficient powder bed spreadability. Due to this poor spreadability, TE powders were either mixed with additives to produce a spreadable slurry or compacted into disks before applying SLM. Thus, it is suggested that powder manufacturing techniques, such as gas atomization (GA), plasma atomization (PA), etc., should be used to produce TE powder with shape characteristics suitable for PBF.

As it is known, materials prepared with SLM are characterized by different metallurgical defects, such as pores and microcracks, and TE materials are no exception, on the contrary, the extent and intensity of such defects are greater due to the nature of TE materials. For example, bismuth telluride is a brittle material with low fracture toughness and low thermal conductivity. The low thermal conductivity of bismuth telluride results in poor heat transfer between the melt pool and the surrounding material during SLM which causes a large temperature gradient leading to intense residual stress [47]. The intense residual stress combined with the low fracture toughness leads to generating microcracks during the SLM of such material.

The physical and mechanical properties of SLMed materials depend significantly on the different mass and heat transport processes within the melting pool. Obtaining detailed knowledge of such processes is important to understand the influence of SLM process parameters. In addition to time-consuming experimental techniques, numerical simulations can assist in generating a sound understanding of the different phenomena and interactions in the melting pool. Limited attempts have been made in the literature to simulate SLM of TE material [96,98]. Therefore, future studies may focus on numerical simulation to attain a comprehensive understanding and overcome the different SLM fabrication challenges of TE material.

3.2. Material extrusion (ME)

ME is an additive manufacturing category in which the starting material is selectively dispensed through a nozzle under the influence of pressure. Direct Ink Writing (DIW) and Fused Deposition Modelling (FDM) are the two main ME processes used for TE materials.

3.2.1. Direct ink writing (DIW)

3.2.1.1. Overview of DIW. DIW, also known as robocasting, is a material extrusion 3D-printing process which uses a nozzle to deposit viscous ink solutions, i.e., slurries or pastes, at a regulated flowrate and temperature over a surface in a layer-by-layer manner [99]. A schematic of DIW is shown in Fig. 13. A TE ink comprises three major ingredients including active TE particles, binder, and solvent. Since the TE particles are normally solid, the ink can be conceived as a solid phase of TE particles dispersed in a matrix phase of the binder. The non-active ingredients of the inks (i.e., binder and solvent) are crucial to enable the inks to have appropriate rheological behaviour, maintain their stability, and facilitate continuous extrusion from the nozzles during the printing process. The concentration of the different ingredients of the ink should be optimized to achieve desirable thermoelectrical properties and good printability. From one side, the ink should have a low viscosity so it can

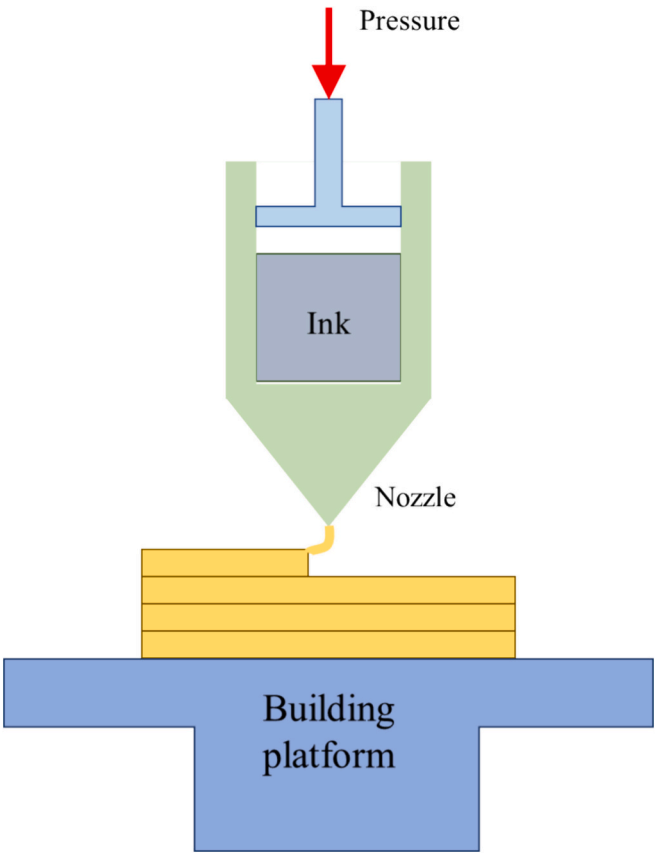

Fig. 13. Schematic of DIW process.

be extruded with less frictional losses and without clogging the extrusion nozzle, thereby improving the productivity of the printing process. On the other side, the ink should solidify quickly after deposition and its post-printing stiffness should be sufficient to enable the 3D shape retention [100]. After the deposition of the ink, the material solidifies either naturally or via an extra process such as heat treatment. Post-deposition treatments have a significant impact on the dimensional accuracy and mechanical properties of the printed object. For TE inks, a post-printing annealing process is normally used to evaporate the excess agents (i.e., binder, reinforcement, solvent, etc.) and sinter the TE particles into a continuous phase.

The flow properties of ink, back pressure, the inner diameter of the nozzle, nozzle translational velocity, and distance between the nozzle and the substrate (standoff distance) are the key parameters for a successful DIW process. The standoff distance determines the layer thickness. This distance is proportional to the inner diameter of the nozzle where it is normally taken as 50%–100% of it [101]. DIW has been successfully used for a wide range of materials including ceramics, polymers, cement, food, and alloys [102,103]. More recently, DIW has received increased applications for TE materials.

3.2.1.2. DIW of TE materials and modules. The earliest studies on DIW of TE materials focused on forming a film (i.e., one layer) of TE material on a substrate. For example, Madan et al. [104] were among the first adopters of dispenser printing to synthesize a thick film of n-type Bi_2Te_3 and p-type Sb_2Te_3 TE materials. The printable inks were formulated by dispersing the semiconductor powders in an epoxy resin system (i.e., polymeric binder) composed of diglycidyl ether of bisphenol f (EPON 862) as the epoxy resin and methylhexahydrophthalic anhydride (MHHPA) as the hardener. The prepared inks were printed on a glass substrate to form films with a thickness ranging from 100 to 200 μm and then cured at different temperatures. The highest ZT values of 0.16 and

0.41 were achieved for Bi_2Te_3 and Sb_2Te_3 when they were cured at 350 °C for 12 h. These measurements for dispenser-printed TE material were higher than those materials prepared by screen-printing processes.

Chen et al. [105] also used dispenser printing to produce TE material and TEG. The TE ink is composed of active TE powder (either n-type Bi_2Te_3 or p-type Sb_2Te_3 particles) and a polymeric binder of a bisphenol-F epoxy resin and an anhydride-based hardener. The printed Bi_2Te_3 and Sb_2Te_3 materials exhibited ZT of 0.18 and 0.19, respectively. The TEG generator was fabricated by using DIW where the n-type and p-type TE materials were deposited on flexible polyimide substrate, as shown in Fig. 14. The TEG was capable of generating 10.5 μW at 171.6 mV for a temperature difference of 20 K.

In another study, Cao et al. [106] used DIW to fabricate 3D TEG. The printed TEG is composed of a flexible polyimide substrate, p-type SbTe thermoleg, n-type BiTe thermoleg, top and bottom silver (Ag) electrodes, and an epoxy structure layer to support the top electrode, as shown in Fig. 15. It was found that the electrical resistance of DIW-printed samples is much higher than those screen-printed thermocouples. The high contact resistance between silver electrodes and the thermoelectric materials was considered the main reason behind the overall high resistance of the 3D-printed TEG.

Shakeel et al. [107] applied DIW to fabricate TEG composed of PEDOT: PSS and silver thermolegs on a glass substrate, as shown in Fig. 16. The materials were extruded through a pneumatic-type 3D printer equipped with a metallic nozzle of 750 μm diameter. Following the printing, the samples were cured at 140 $^{\circ}C$ for 30 min to remove any solvent. The printed TEG yielded a maximum power of 5.17 ± 0.5 nW at a temperature difference of 120 $^{\circ}C$.

Du et al. [108] used DIW to prepare mechanically flexible double-layer TE material. Two composites inorganic/organic layers of Ag/PLA and Bi_2Te_3-based alloy (BTBA)/PLA are used. The solution used for BTBA/PLA is prepared by dissolving 0.5 g PLA in 5 mL chloroform and then mixing the obtained solution with 2 g of BTBA. Ag/PLA solution is obtained by mixing an appropriate amount of Ag with a solution prepared by dissolving 0.5 g PLA in 5 mL chloroform. The additive manufacturing process was completed by printing the BTBA/PLA solution on a glass substrate to form the BTBA/PLA layer, after that the Ag/PLA solution was printed on the BTBA/PLA layer to form the double-layer material. A nozzle diameter of 0.5 mm and a printing speed of 300 $mm.min^{-1}$ were used as printing process parameters. The chloroform was evaporated as the last step before obtaining the double-layer TE material. The double-layer material with 41.7 vol% of Ag exhibited the best TE performance represented by a power factor of 875 $\mu W\ m^{-1}\ K^{-2}$ at 360 K.

Du et al. [109] assessed the TE performance of AMed n-type tungsten carbide/polylactic acid (WC/PLA) composites. To prepare WC/PLA ink, 0.8 g of PLA was first dissolved in 12 mL of chloroform and then the formulated solution was mixed with an appropriate amount of WC to produce the final viscous printable ink. The 3D printing process started by inhaling the ink into the syringes and then depositing it through a nozzle with a diameter of 5 mm at a flow speed of 300 $mm.min^{-1}$. The deposited material was dried at 60 °C for 12 h where the chloroform was evaporated, and the WC/PLA composite was formed. The AMed WC/PLA composite with a mass ratio of 15:0.8 yielded the highest ZT value of $\sim 6.7 \times 10^{-4}$ at 300 K; and exhibited good flexibility and stability. Therefore, the fabricated composite was considered suitable for flexible TE devices.

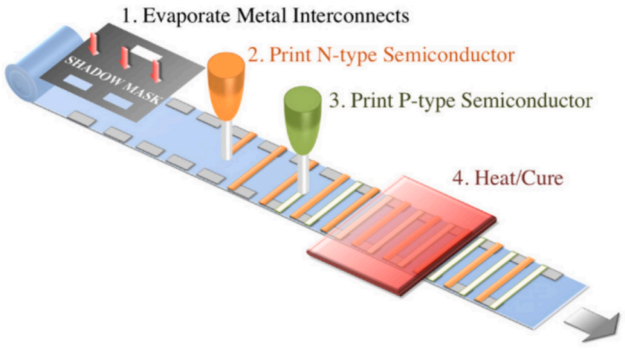

Fig. 14. 3D-printing of TEG using DIW [105].

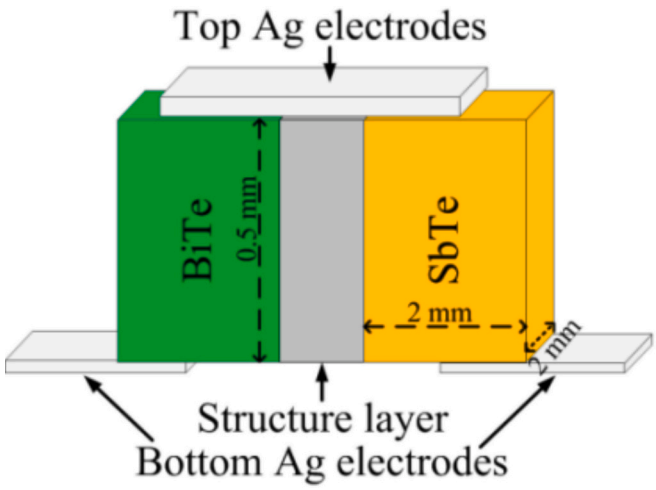

Fig. 15. Illustration of a 3D-printed thermocouple with the electrodes and support structure [106].

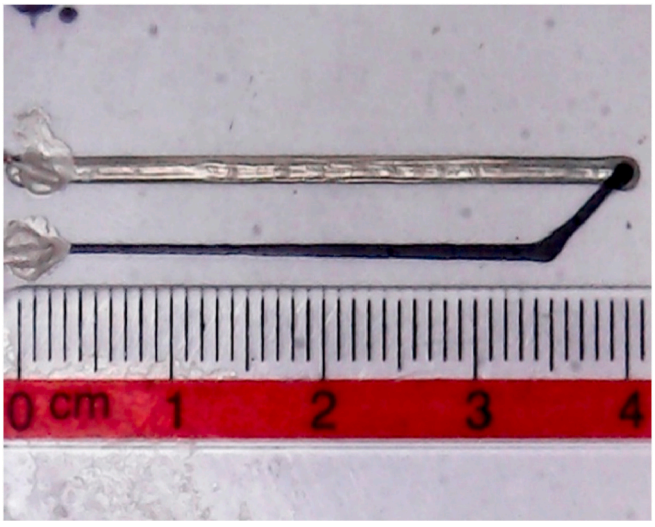

Fig. 16. DIW-printed TEG with PEDOT:PSS and silver legs [107].

Du et al. [110] used DIW to prepare flexible ternary carbon black/Bi_2Te_3-based alloy/polylactic acid (CB/BTBA/PLA) TE composites. It was found that both electrical conductivity and Seebeck coefficient increase as the mass ratio of BTBA in the composite increases. The highest ZT value of 0.024 was obtained at 320 K for the CB/BTBA/PLA TE composite with a 71.4% mass ratio of BTBA.

Hwang et al. [111] fabricated carbon TE materials and TEGs by utilizing DIW. The printable ink consisted of thermoelectric particles of Single-Walled Carbon Nanotubes (SWCNTs), a solvent of diethylene glycol (DEG) and polymeric binders of p-type poly(acrylic acid) (PAA) and n-type poly(ethylenimine) (PEI). The concentrations of the ink ingredients were optimized to ensure suitable rheological properties and continuous extrusion from the nozzles during the printing process. The n-type SWCNT/PAA material with 30 wt% concentration of PAA exhibited a power factor of 235.05 $\mu Wm^{-1}\ K^{-2}$. On the other side, the p-

type SWCNT/PEI material with 18 w.% concentration of PEI yielded the highest power factor of 200.17 $\mu Wm^{-1} K^{-2}$. The 3D printed TEG with 35 thermoelectric pairs produced a power of 288.33 nW and provided an open-circuit voltage of 39.18 mV at ΔT of 15 K. The study also proved that the DIW-fabricated materials provide better TE properties than blad-casted material.

Kee et al. [112] fabricated stretchable and self-healing wearable TEGs using DIW of a ternary composite of PEDOT:PSS blended with a polymeric surfactant as a soft matrix, dime-thyl sulfoxide (DMSO) as a thermoelectric performance booster, and Triton X-100 as a healing agent. The DIW-fabricated TEG yielded an electrical output of 12.2 nW. Interestingly, the TEG retained approximately 85% of its power output after inducing damage through repetitive cutting.

In all the above studies, organic binders were employed in the TE inks to enhance the viscoelastic behaviour and printability. However, the intrinsic poor electrical conductivity of such organic compounds will inevitably degrade the thermoelectric performance of the final printed material. Therefore, many studies attempted to prepare printable inks with all inorganic ingredients. Kim et al. [113] fabricated TE material with complex geometries, suitable for the shape of heat sources, using inorganic viscoelastic inks composed of Sb_2Te_3 chalcogenidometallate (ChaM) ions as inorganic binders and Bi_2Te_3 as TE particles. The printed material exhibited good TE measurements with ZT of 0.9 and 0.6 for p- and n-type, respectively. Kim et al. [114] expanded the previous work by using DIW to fabricate a high-performance micro thermoelectric generator (μ-TEG) with $Bi_{0.5}Sb_{1.5}Te_3$ and $Bi_2Te_{2.7}Se_{0.3}$ as p-type and n-type legs, respectively. The TE legs were directly printed on Ag electrodes which were screen-printed on a Si/SiO_2 substrate. The TE inks consisted of the TE powder with an inorganic binder of Sb_2Te_4 ChaM and a solvent of glycerol. The 3D-printed n-type and p-type materials offered ZT values of 0.37 and 0.92, respectively. The 3D-printed μ-TEG exhibited a maximum output voltage of 42.4 mV, a power of 2.8 μW, and a power density of 479.0 $\mu W\ cm^{-2}$ at a temperature difference of 82.9 °C. Such power density is enough to power advanced wireless sensor networks.

Eom et al. [100] investigated the rheological properties of BiSbTe-based TE ink that uses ChaM as an inorganic binder. Bi, Sb, and Te granules were first ball-milled and then sieved to obtain Bi_2Te_3-based TE powder with appropriate particle size. The ink was synthesized by adding 2 g of the TE powder and the desirable amount of ChaM dispersed in 2 g of glycerol. A pneumatic extrusion-based 3D printer with a nozzle diameter of 260 μm was used as the printing system. The 3D printing process was conducted with a speed of 18 $mm.s^{-1}$ and a pressure of 0.34 MPa. The ink containing 25 wt% ChaM exhibited stable flow behaviour and good printability resulting in high structure integrity of the 3D-printed material.

Wang et al. [115] synthesized water-based quasi-inorganic inks and then used them to fabricate n-type $Bi_2Te_3Se_{0.3}$ and p-type $Bi_{0.5}Sb_{1.5}Te_3$ TE materials by DIW process. The inks contained 65–85 wt% of TE particles with very small amounts of organic composites (PAA and PEI) as binder and deionized water as solvent. The printed samples were dried at room temperature for 24 h and then annealed at 450°C for 2 h in an inert environment to remove any remaining organic compounds as well as consolidate the TE particles. The DIW-prepared material showed excellent TE performance yielding maximum ZT values of 0.71 and 0.59 for p-type and n-type, respectively. TEG was also assembled from three pairs of additively manufactured p- and n-type legs with half-annular shapes connected in series using Cu electrodes. The TEG provided maximum electrical output of 0.38 mW for a temperature difference of 55 K.

Wang et al. [116] formulated DIW-printable inks from TE particles with polyelectrolyte additives including anionic PAA and cationic PEI as well as methylcellulose (MC) reinforcement, as can be seen in Fig. 17. The ink with 0.9 wt% MC and 70.2 wt% TE loading exhibited very good viscoelasticity, enhanced mechanical properties, extrusion stability and printability, and excellent structural recovery. The DIW-printed p-type $Bi_{0.5}Sb_{1.5}Te_3$ and n-type $Bi_2Te_3Se_{0.3}$ TE materials using this ink showed very good thermoelectrical properties including ZT values of 0.65 and 0.53, respectively.

3.2.1.3. Challenges and prospects of DIW for TE materials. DIW is a simple, cost-effective, and versatile method that offers many advantages over other AM technologies. First, DIW has the capability to produce the whole TEM as it is suitable for multi-material printing through separate

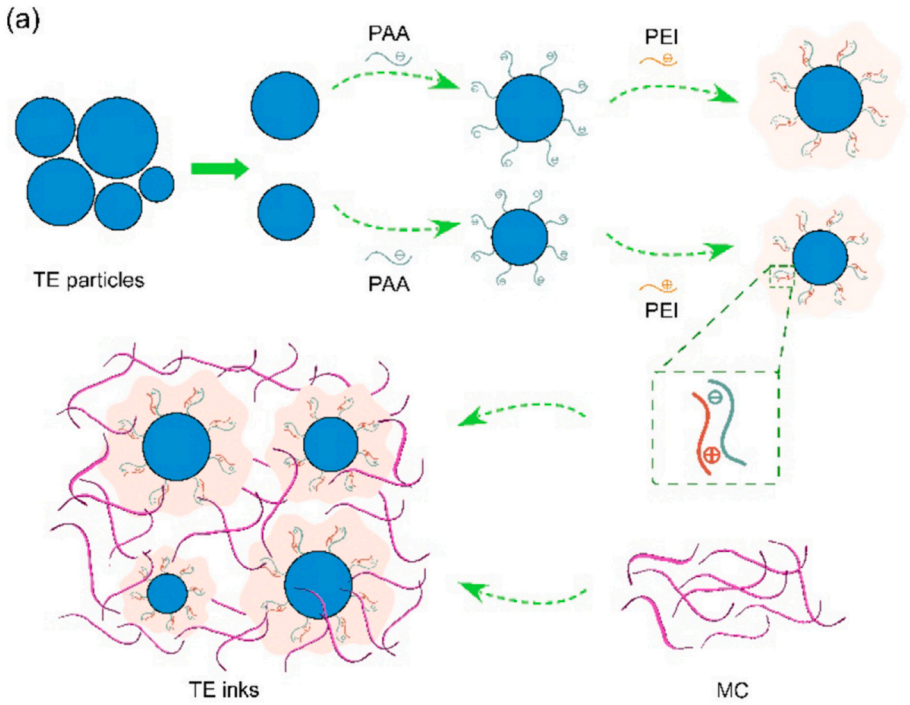

Fig. 17. Schematic of DIW-printable TE inks containing TE particles, PAA and PEI additives, and MC reinforcement [116].

and simultaneous extrusion of different TE slurries [102]. Also, unlike FDM and SLM, DIW takes place at the ambient temperature without heating the feedstock (ink) making it an energy-efficient process and reducing the potential of material oxidation [45]. Furthermore, DIW is not restricted by material type as long as the ink has viscoelastic properties [102]. Similar to inkjet and screen printing technologies, DIW is attractive for fabricating Flexible Thermoelectric Modules (FTM) due to its simplicity and reduced energy input and waste [13,105]. DIW can be used to realize FTM through two main approaches. One approach is about using DIW to print rigid inorganic TE materials, such as Bi_2Te_3 and Sb_2Te_3, on flexible substrates. The second approach involves employing DIW to print flexible organic TE materials, such as PEDOT:PSS, and PANI [49].

Preparing well-formulated, stable, and printable ink is the primary obstacle of DIW technology. The composition, wettability, and viscoelastic properties of the ink are the main factors affecting the DIW process. The ink should have suitable concentrations of the solid and liquid phases to balance the rheological behaviour, during printing, with the thermoelectric properties and mechanical stability, after printing. The end properties of the ink are sensitive to the characteristics of its ingredients such as particle size and shape, and concentration of the solid particles. For example, the high concentration of solid particles will cause aggregation of the solid particles in the ink which might clog the nozzle during the printing and at the same time increase the pressure required to induce flow. For the TE inks, the solid particles are mostly obtained by grinding or crushing bulk ingots and therefore their morphology might not be the best for preparing a well-formulated ink.

The low dimensional accuracy and geometrical defects are other challenges for the DIW-fabricated parts. Normally, shrinkage takes place during the curing of the deposited ink which might cause the warpage of the final part [117].

Another disadvantage of DIW is that it is relatively slow, compared to other AM methods such as PBF, due to the limited translational velocity of the nozzle ($\sim 1-20\ mm.s^{-1}$) that can be used during the printing. The high relative speed between the nozzle and the substrate can cause different forms of manufacturing defects such as discontinued lines, bulging, liquid puddles, and liquid splashing [101,118]. Therefore, DIW is considered to be unsuitable for mass production of TE materials. Recently, a novel approach represented by using an electric field to facilitate DIW with electrohydrodynamic jetting has been used and resulted in increasing the printing speed to 500 $mm.s^{-1}$ [101].

3.2.2. Fused deposition modelling (FDM)

3.2.2.1. Overview of FDM. FDM, also termed Fused Filament Fabrication (FFF), is an extrusion-based 3D printing technique in which filament feedstock is selectively extruded via a nozzle or orifice to build the part layer-by-layer, as shown in Fig. 18. FDM is mainly used to additively manufacture thermoplastic polymers, such as Acrylonitrile Butadiene Styrene (ABS), Polylactic Acid (PLA), Polyvinyl Alcohol (PVA), Nylon, and Polyimide (PA), as well as Fibre Reinforced Thermoplastics Composites (FRTC), such as carbon fibre reinforced PLA composites [119–121].

The extruder in FDM systems consists of a liquefier chamber and nozzle. During the printing process, the feeder wheels push the filament into a liquified chamber where the material melts and then flows out the nozzle tip due to the pressure difference between the chamber and the surrounding atmosphere [122]. Subsequently, the extruded molten material solidifies and bonds with the adjacent materials. The position control system of the FDM machine controls the motion of both the extruder head and the building platform. The extruder head moves in the horizontal plane, to control the deposition path of the material, while the building platform moves vertically to build the individual layers. The main process parameters that influence the quality and mechanical properties of the FDM-built part are deposition speed (feed rate), layer thickness, nozzle diameter, infill density, fill pattern, building orientation, extrusion temperature, and platform temperature [120]. The building platform is heated sometimes to improve the adhesion with the extruded material and also to reduce the possible defects in the printed part [123].

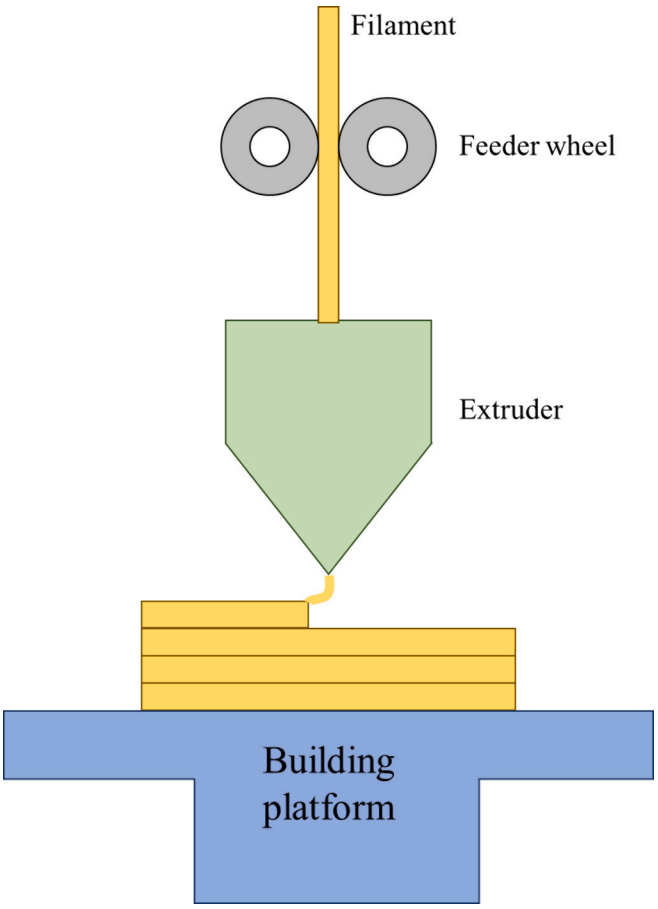

Fig. 18. Schematic of FDM process.

3.2.2.2. FDM of TE materials. Oztan et al. [16] prepared Bi_2Te_3 TE material by FFF. The filament, used in the FFF process, was obtained by extruding a mixture composed of 80% Bi_2Te_3 powder with 20% ABS polymer powder. The filament was then deposited on a building base through a nozzle with a diameter of 0.4 mm. The temperatures of the nozzle and the building base were maintained at 260°C and 90°C, respectively. The printed material was then sintered to remove the polymer matrix and fuse any remaining Bi_2Te_3 particles. The as-printed FFF-fabricated material demonstrated a compression strength of 46.53 MPa while the material sintered at 500°C yielded 40% less compression strength (33.14 MPa). The sintering temperature has an influence on all thermoelectric properties of the printed samples, as can be seen in Fig. 19. The maximum ZT of 0.54 at room temperature was achieved for samples sintered at 500°C. Authors reported that the FFF process can produce TE material with ZT higher than those materials prepared by SLA printing or dispenser printing.

AW et al. [124] studied the influence of FDM process parameters, including infill density and printing pattern, on the mechanical and thermoelectric properties of conductive acrylonitrile butadiene styrene/zinc oxide (CABS/ZnO) thermoelectric composites containing 14 wt% ZnO. It was found that the tensile strength and dynamic storage modulus increase while the loss modulus and damping factor reduce as the infill density increases. The as-printed composite exhibited low electrical conductivity and Seebeck coefficient. The highest ZT value of $\sim 5.7\times$

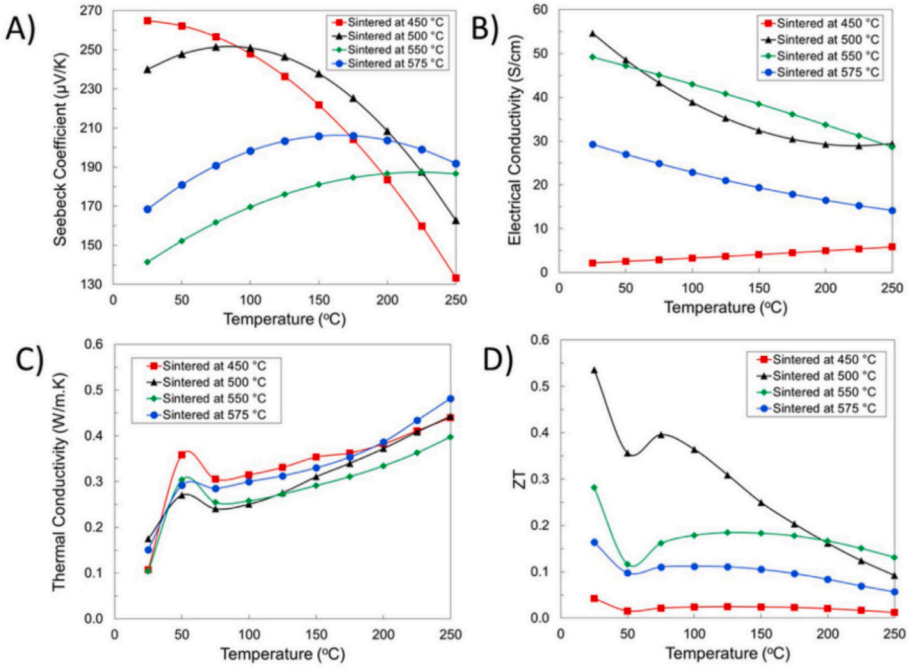

Fig. 19. TE properties of FFF-fabricated Bi_2Te_3 [16].

10^{-5} was obtained for material fabricated with 100% infill and line printing pattern.

Wang et al. [125] investigated the TE and mechanical properties of PLA/$Bi_{0.5}Sb_{1.5}Te_3$ composite wires that can be used as feedstock in the FDM process. The composite wires were obtained by extruding PLA powder as the matrix, $Bi_{0.5}Sb_{1.5}Te_3$ powder as the filler, Multi-Wall Carbon Nano Tubes (MWCNTs) as the conductive additive, and 3-(Trimethoxysilyl)propyl methacrylate as the coupling agent. The composite containing 4 wt% MWCNTs and 81.3 wt% $Bi_{0.5}Sb_{1.5}Te_3$ exhibited the best TE performance of PF = 11.3 μW m^{-1} K^{-2} and ZT = 0.011 at room temperature.

3.2.2.3. Challenges and prospects of FDM for TE materials. Given that the FDM process uses heat with temperatures up to 200°C, oxidation might take place for the FDM-fabricated inorganic TE materials such as PbTe- and BiTe-based alloys. Oxidation is a significant concern for TE materials because it damages both the mechanical and thermoelectric performance. Oxides have high thermal conductivity and low electrical conductivity so they reduce ZT performance when exist within the TE materials [126]. The oxides are also brittle and have a high cracking probability; therefore, they can cause mechanical failure of the TE materials during operation [40]. Using a protective atmosphere might be an effective solution to minimize oxidation during the FDM process.

The low electrical conductivity of the filament is another challenge for adopting FDM for TE materials. The filaments normally contain high polymeric content which restricts their electrical conductivity [127].

3.3. Vat Photopolymerization (VP)

3.3.1. Overview of VP

VP AM processes use either visible or ultraviolet (UV) light to induce a photochemical reaction, known as photopolymerization, in which photosensitive resins (i.e., light-curable photopolymers) solidify or harden creating the part layer-by-layer [122]. The photochemical reaction simply links the small monomers within the liquid photopolymer together to form a chain-like polymer structure [128]. Compared to other AM technologies, VP processes provide the advantages of cost-effectiveness, high accuracy, and fast building.

The light sources, used in VP, can be in different forms such as lamps, LEDs, or lasers with different wavelengths ranging from UV to visible to infrared (IR) depending on the type of photoinitiator [129,130]. The photopolymers, used in VP, are materials that change their chemical and physical properties when they are subjected to light. Photopolymers are composed of different ingredients such as photoinitiators, flexibilizers, liquid monomers, reactive diluents, and stabilizers [131]. (Meth)acrylate-based resins (such as PEGDA, TEGDMA, Bis-GMA, Bis-EDA, and TTA), Thiol–ene-based resins (such as TMPMP, PETMP, and PE-1), cationic systems (such as EPOX, DSO, DGEBA, and CDVE) are frequently used as 3D printable photopolymers [129].

Digital Light Processing (DLP), Stereo Lithography (SLA), and Continuous liquid interface Production (CLIP) are the three main technologies of VP. DLP is a layer-wise, or mask projection, approach in which a digital mask, known as Digital Micromirror Device (DMD), is used to project the light onto the resin surface, thereby creating an entire layer at once [132]. Unlike DLP, SLA is a point-wise, or vector scan, approach in which an optical scanning module is used to selectively focus the light on specific points of the resin surface curing the resin point-by-point, as illustrated in Fig. 20. Contrary to the layer-by-layer approach used in SLA and DLP, CLIP is a VP process that fabricates a 3D part continuously without interruption. CLIP uses a dead zone that contains atmospheric oxygen to prevent the photopolymerization process and maintain a liquid interface below the fabricated part [131]. During DLIP, a digital light-processing imaging unit projects UV images on the dead zone while simultaneously the cured part above the dead zone is drawn out of the resin vat enabling the continuous fabrication process [133].

3.3.2. VP of TE materials

He et al. [134] fabricated p-type $Bi_{0.5}Sb_{1.5}Te_3$ TE materials by using SLA. Composite resins, containing TE powders, Formlabs clear photoresins, and customized epoxy resin, were used in the SLA process. Post-printing thermal treatment was conducted to remove the photoresins from the printed samples. It was shown that the thermal treatment enables achieving a single-phase of $Bi_{0.5}Sb_{1.5}Te_3$ in the printed material. However, the annealing process caused the decomposition of photoresins and generated amorphous carbons within the annealed material.

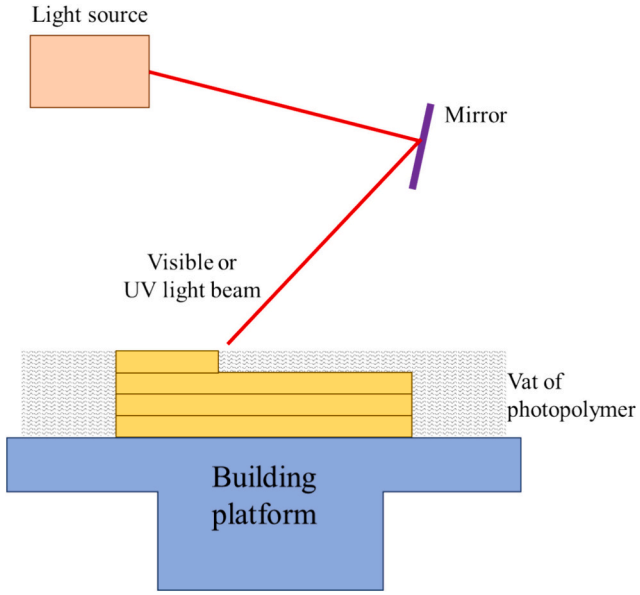

Fig. 20. Schematic of SLA process.

The decomposition of the photoresins increased the porosity in the annealed samples compared to untreated samples. The best ZT value of 0.12 was achieved at 43 °C for a sample with 60 wt% of TE particles and annealed at 350 °C for 6 h.

3.3.3. Challenges and prospects of VP for TE materials

Application of SLA for fabricating TE materials is somewhat limited as most of photoresins used in SLA have low electrical conductivity which in turn reduces the ZT values of the SLA-processed material.

One advantage of SLA is its multi-material printing capability which allows it to fabricate the complete TEM with both n- and p-type legs. However, multi-material printing is still impractical using SLA as it requires changing the resin in the vat and aligning the surface of the liquid with the processed solid segment.

Despite that SLA generates good surface quality compared to FDM, the scanned lines, during SLA, sometimes appear and cause ribbing for the surface of the processed materials resulting in low surface quality and high surface roughness. Such low surface quality is unfavourable for TEM as it increases the thermal and electrical contact resistances leading to decreasing the overall thermoelectric performance.

SLA uses a post-printing thermal annealing step to remove the photosensitive resin and to coalesce the TE solid particles. However, the annealing parameters depend on the type of materials and therefore it is challenging to design an SLA process that works for all types of TE materials.

4. Conclusion

Thermoelectric technologies play a key role in achieving a sustainable energy solution via the direct conversion of heat into electricity. To date, the industrial applications of TE technologies are limited to some niche areas and not commercialized widely. The high material cost and manufacturing challenges are the critical barriers to the large-scale commercialization of TE technologies.

This paper provided a detailed overview of the research advancements on the applications of additive manufacturing technologies for fabricating thermoelectric materials and devices and summarized their advantages and challenges.

As a digital manufacturing approach, AM creates significant opportunities to revolutionize TE technologies and provide key technical, economical, and environmental advantages at material and system levels. At the material level, AM technologies provide the ability to prepare high-performance TE material with complexly shaped morphologies and controlled microstructures that can reduce the thermal conductivity of the material through phonon scattering without compromising the electrical conductivity. Additionally, AM, with its layer-by-layer construction approach, maximizes material utilization and reduces the wastage of raw TE materials. This is particularly beneficial for either expensive and scarce TE materials, such as bismuth telluride-based materials, or TE materials with toxic elements, such as lead-based materials. Furthermore, some AM techniques, particularly those operating at ambient temperature, have lower cost and energy consumption than traditional manufacturing approaches, such as zone melting, hot pressing or spark plasma sintering, where high pressure and temperature are essential process parameters. At the system level, AM can facilitate one-step manufacturing of TE devices at lower costs. Also, AM facilitates the integration of different parts within the TE device reducing the number of parts required for it. Furthermore, AM can fabricate intricately shaped thermoelectric devices with optimized dimensions and geometry that perfectly conform to the shape of the heat source. Such shape conformity yields better thermal dissipation and improves the electrical power output compared to conventional planar devices.

Despite the high potential of AM for TE materials fabrication, many challenges still need to be addressed. The performance of AM-manufactured TE materials is still lower than the CM-prepared counterparts due to many inherent shortcomings of AM technologies. The surface quality of the AMed materials is generally not very good. AM processes normally produce rough surfaces due to the layer-by-layer nature of the processes and the staircase effects. The rough surfaces are not desirable for TE materials because they increase contact resistance and degrade the crack and corrosion resistance of the material. Enhancing the surface quality of AMed TE materials requires optimizing the process parameters such as building direction, layer thickness, etc. In addition to low surface quality, many of the AM processes, such as SLM and SLA, are known to generate some porosity within the produced materials. Despite that the porosity might be beneficial in reducing the thermal conductivity, its negative influence on mechanical properties and electrical conductivity is also considerable and may lead to lower overall TE performance. Furthermore, due to the nature of AM techniques, AMed TE materials have anisotropic thermoelectric properties where such properties are sensitive to the printing direction. The anisotropy of the AMed TE materials can make the design of the thermoelectric devices more complicated and limit their maximum efficiency.

While the thermoelectric properties of AMed TE materials have received acceptable studies, their mechanical properties, such as stiffness, bending strength, compressive strength, fracture toughness, and hardness, have received less investigation. The comprehensive knowledge of mechanical properties is critical to estimate the ability of TE materials to withstand the service conditions and to advance the practical application of the technologies. Thus, future research is required to reveal all the important mechanical properties of TE materials.

The performance of AMed TE materials depends not only on the material composition but also on the parameters of the printing process and the subsequent heat treatment. The optimization of these parameters to achieve the optimal TE output has received limited research attention and requires wider exploration. In this respect, the application of machine learning approaches could be significantly beneficial to explore the influence of a wide range of parameters on the important TE characteristics.

The sustainability performance of AMed thermoelectric materials is another area that requires further studies because only limited attention was given in the literature to performing Life Cycle Assessment (LCA) and assessing the environmental impact of such materials.

The additive manufacturing technologies have emerged at the right time to tackle the scalability and performance issues of thermoelectric

devices. AM technologies are going through massive research investigations which can only result in addressing the major obstacles associated with their applications for TE materials.

Nomenclature

$\dot{Q}_h$	Heating power (W)
$\dot{Q}_c$	Cooling power (W)
E_A	Areal energy density $(J.m^{-2})$
E_L	Linear energy density $(J.m^{-1})$
E_V	Volumetric energy density $(J.m^{-3})$
P_{elec}	Electrical power (W)
P_{laser}	Laser power (W)
$\dot{Q}$	Thermal power (W)
R_H	Hall coefficient $(m^3.C^{-1})$
m^*	Carrier effective mass (kg)
h	Hatch distance (m)
CoP	Coefficient of Performance
I	Electrical current (A)
PF	Power factor $(W.m^{-1}.K^2)$
S	Seebeck coefficient $(V.K^{-1})$
T	Temperature (K)
ZT	Thermoelectric figure-of-merit
n	Carrier concentration (m^{-3})
t	Layer thickness (m)
v	Scanning speed $(m.s^{-1})$
κ_E	Electronic thermal conductivity $(W.m^{-1}.K^{-1})$
κ_L	Lattice thermal conductivity $(W.m^{-1}.K^{-1})$
ΔT	Temperature gradient (K)
ΔV	Electrical voltage (V)
Π	Peltier coefficient (V)
η	Efficiency
κ	Thermal conductivity $(W.m^{-1}.K^{-1})$
μ	Carrier mobility $(m^2.V^{-1}.s^{-1})$
ρ	Electrical resistivity $(\Omega.m)$
3DP	Three-Dimensional Printing
AM	Additive Manufacturing
CLIP	Continuous liquid interface Production
CM	Conventional Manufacturing
DIW	Direct Ink Writing
DLP	Digital Light Processing
DMD	Digital Micromirror Device
ED	Energy Density
FDM	Fused Deposition Modelling
ME	Material Extrusion
PBF	Powder Bed Fusion
SLA	Stereo Lithography
SLM	Selective Laser Melting
TE	Thermoelectric
TEC	Thermoelectric Cooler
TEG	Thermoelectric Generator
TEM	Thermoelectric Module
UV	Ultraviolet
VP	Vat Photopolymerization
WHR	Waste Heat Recovery

Constants

k_B	Boltzmann constant ($k_B = 1.380649 \times 10^{-23} (J.K^{-1})$)
h	Planck constant ($h = 6.62607015 \times 10^{-34} (J.HZ^{-1})$)
e	Elementary charge ($e = 1.60217663 \times 10^{-19} (C)$)
L	Lorenz number ($L = 2.44 \times 10^{-8} (V^2K^{-2})$)

CRediT authorship contribution statement

Ahmad Baroutaji: Conceptualization, Formal analysis, Investigation, Methodology, Writing – original draft, Writing – review & editing, Validation. **Arun Arjunan:** Conceptualization, Formal analysis, Investigation, Methodology, Writing – review & editing. **John Robinson:** Conceptualization, Formal analysis, Investigation, Methodology, Writing – review & editing. **Mohamad Ramadan:** Conceptualization, Formal analysis, Investigation, Methodology, Writing – review & editing. **Mohammad Ali Abdelkareem:** Conceptualization, Formal analysis, Investigation, Methodology, Writing – review & editing. **Aaron Vance:** Conceptualization, Formal analysis, Investigation, Methodology, Writing – review & editing. **Abul Arafat:** Conceptualization, Formal analysis, Investigation, Methodology, Writing – review & editing. **Abdul-Ghani Olabi:** Conceptualization, Formal analysis, Investigation, Methodology, Writing – review & editing.

Declaration of competing interest

The authors declare that they have no known competing financial interests or personal relationships that could have appeared to influence the work reported in this paper.

Data availability

Data will be made available on request.

References

[1] R. Fitriani, B.D. Ovik, M.C.M. Long, M. Barma, M.F.M. Riaz, S.M.S.M. Sabri, R. Said, Saidur, a review on nanostructures of high-temperature thermoelectric materials for waste heat recovery, Renew. Sust. Energ. Rev. 64 (2016) 635–659, https://doi.org/10.1016/J.RSER.2016.06.035.

[2] H. Jouhara, A.G. Olabi, Editorial: industrial waste heat recovery, Energy 160 (2018) 1–2, https://doi.org/10.1016/j.energy.2018.07.013.

[3] H. Jouhara, N. Khordehgah, S. Almahmoud, B. Delpech, A. Chauhan, S.A. Tassou, Waste heat recovery technologies and applications, Therm. Sci. Eng. Prog. 6 (2018) 268–289, https://doi.org/10.1016/j.tsep.2018.04.017.

[4] S. Twaha, J. Zhu, Y. Yan, B. Li, A comprehensive review of thermoelectric technology: materials, applications, modelling and performance improvement, Renew. Sust. Energ. Rev. 65 (2016) 698–726, https://doi.org/10.1016/J.RSER.2016.07.034.

[5] S. Leblanc, S.K. Yee, M.L. Scullin, C. Dames, K.E. Goodson, Material and manufacturing cost considerations for thermoelectrics, Renew. Sust. Energ. Rev. 32 (2014) 313–327, https://doi.org/10.1016/j.rser.2013.12.030.

[6] N. Jaziri, A. Boughamoura, J. Müller, B. Mezghani, F. Tounsi, M. Ismail, A comprehensive review of thermoelectric generators: technologies and common applications, Energy Rep. 6 (2020) 264–287, https://doi.org/10.1016/J.EGYR.2019.12.011.

[7] H. Jouhara, A. Zabnie Nska-G Ora, N. Khordehgah, Q. Doraghi, L. Ahmad, L. Norman, B. Axcell, L. Wrobel, S. Dai, A. Żabnieńska-Góra, N. Khordehgah, Q. Doraghi, L. Ahmad, L. Norman, B. Axcell, L. Wrobel, S. Dai, Thermoelectric generator (TEG) technologies and applications, Int. J. Thermofluids 9 (2021) 100063, https://doi.org/10.1016/j.ijft.2021.100063.

[8] A. Baroutaji, A. Arjunan, M. Ramadan, J. Robinson, A. Alaswad, M. A. Abdelkareem, A.G. Olabi, Advancements and prospects of thermal management and waste heat recovery of PEMFC, Int. J. Thermofluids 9 (2021) 100064, https://doi.org/10.1016/j.ijft.2021.100064.

[9] I. Terasaki, Introduction to thermoelectricity, in: Mater. Energy Convers. Devices a Vol. Woodhead Publ. Ser. Electron. Opt. Mater, 2005, pp. 339–357, https://doi.org/10.1533/9781845690915.3.339.

[10] S.H. Zaferani, M.W. Sams, R. Ghomashchi, Z.-G. Chen, Thermoelectric coolers as thermal management systems for medical applications: design, optimization, and advancement, Nano Energy 90 (2021), https://doi.org/10.1016/j.nanoen.2021.106572.

[11] N. Nandihalli, C.-J. Liu, T. Mori, Polymer based thermoelectric nanocomposite materials and devices: fabrication and characteristics, Nano Energy 78 (2020) 105186, https://doi.org/10.1016/j.nanoen.2020.105186.

[12] I. Terasaki, Thermal conductivity and thermoelectric power of semiconductors, Compr. Semicond. Sci. Technol. 1–6 (2011) 326–358, https://doi.org/10.1016/B978-0-44-453153-7.00070-5.

[13] M. Orrill, S. LeBlanc, Printed thermoelectric materials and devices: fabrication techniques, advantages, and challenges, J. Appl. Polym. Sci. 134 (2017), https://doi.org/10.1002/app.44456.

[14] M.J. Kruszewski, L. Ciupinski, R. Zybala, Review of rapid fabrication methods of skutterudite materials, Mater. Today Proc. 44 (2021) 3475–3482, https://doi.org/10.1016/J.MATPR.2020.05.808.

[15] J. Shi, H. Chen, S. Jia, W. Wang, Rapid and low-cost fabrication of thermoelectric composite using low-pressure cold pressing and thermocuring methods, Mater. Lett. 212 (2018) 299–302, https://doi.org/10.1016/j.matlet.2017.10.087.

[16] C. Oztan, S. Ballikaya, U. Ozgun, R. Karkkainen, E. Celik, Additive manufacturing of thermoelectric materials via fused filament fabrication, Appl. Mater. Today 15 (2019) 77–82, https://doi.org/10.1016/j.apmt.2019.01.001.

[17] S. LeBlanc, Thermoelectric generators: linking material properties and systems engineering for waste heat recovery applications, sustain, Mater. Technol. 1 (2014) 26–35, https://doi.org/10.1016/j.susmat.2014.11.002.

[18] A. Charles, A. Hofer, A. Elkaseer, S.G. Scholz, Additive manufacturing in the automotive industry and the potential for driving the green and electric transition, smart Innov, Syst. Technol. 262 (2022) 339–346, https://doi.org/10.1007/978-981-16-6128-0_32/COVER.

[19] H. Fu, S. Kaewunruen, State-of-the-art review on additive manufacturing technology in railway infrastructure systems, J. Compos. Sci. 6 (2022) 7, https://doi.org/10.3390/JCS6010007.

[20] B. Blakey-Milner, P. Gradl, G. Snedden, M. Brooks, J. Pitot, E. Lopez, M. Leary, F. Berto, A. du Plessis, Metal additive manufacturing in aerospace: a review, Mater. Des. 209 (2021) 110008, https://doi.org/10.1016/J.MATDES.2021.110008.

[21] D. Delgado Camacho, P. Clayton, W.J. O'Brien, C. Seepersad, M. Juenger, R. Ferron, S. Salamone, Applications of additive manufacturing in the construction industry – a forward-looking review, Autom. Constr. 89 (2018) 110–119, https://doi.org/10.1016/j.autcon.2017.12.031, accessed May 17, 2023.

[22] R. Kumar, M. Kumar, J.S. Chohan, The Role of Additive Manufacturing for Biomedical Applications: A Critical Review, 2021.

[23] M.P. Chhaya, P.S.P. Poh, E.R. Balmayor, M. Van Griensven, J.T. Schantz, D. W. Hutmacher, Additive manufacturing in biomedical sciences and the need for definitions and norms 12 (2015) 537–543, https://doi.org/10.1586/17434440.2015.1059274.

[24] I. Kaur, P. Singh, State-of-the-art in heat exchanger additive manufacturing, Int. J. Heat Mass Transf. 178 (2021), https://doi.org/10.1016/j.ijheatmasstransfer.2021.121600.

[25] J. Sun, Z. Peng, W. Zhou, J.Y.H. Fuh, G.S. Hong, A. Chiu, A review on 3D printing for customized food fabrication, Proc. Manuf. 1 (2015) 308–319, https://doi.org/10.1016/J.PROMFG.2015.09.057.

[26] A.H. Alami, A. Ghani Olabi, S. Khuri, H. Aljaghoub, S. Alasad, M. Ramadan, M. A. Abdelkareem, 3D printing in the food industry: recent progress and role in achieving sustainable development goals, Ain Shams Eng. J. (2023), https://doi.org/10.1016/j.asej.2023.102386.

[27] Y.L. Yap, W.Y. Yeong, Additive manufacture of fashion and jewellery products: a mini review, Virtual Phys. Prototyp. 9 (2014) 195–201, https://doi.org/10.1080/17452759.2014.938993.

[28] S.M.H. Hashemi, U. Babic, P. Hadikhani, D. Psaltis, The potentials of additive manufacturing for mass production of electrochemical energy systems, Curr. Opin. Electrochem. 20 (2020) 54–59, https://doi.org/10.1016/J.COELEC.2020.02.008.

[29] C. Sun, Y. Wang, M.D. McMurtrey, N.D. Jerred, F. Liou, J. Li, Additive manufacturing for energy: a review, Appl. Energy 282 (2021) 116041, https://doi.org/10.1016/J.APENERGY.2020.116041.

[30] A. Baroutaji, A. Arjunan, J. Robinson, M.A. Abdelkareem, A.G. Olabi, Additive manufacturing for proton exchange membrane (PEM) hydrogen technologies: merits, challenges, and prospects, Int. J. Hydrog. Energy 52 (2023) 561–584, https://doi.org/10.1016/j.ijhydene.2023.07.033.

[31] S. Ford, M. Despeisse, Additive manufacturing and sustainability: an exploratory study of the advantages and challenges, J. Clean. Prod. 137 (2016) 1573–1587, https://doi.org/10.1016/j.jclepro.2016.04.150.

[32] T. Peng, K. Kellens, R. Tang, C. Chen, G. Chen, Sustainability of additive manufacturing: An overview on its energy demand and environmental impact, Addit. Manuf. 21 (2018) 694–704, https://doi.org/10.1016/j.addma.2018.04.022.

[33] S.H. Huang, P. Liu, A. Mokasdar, L. Hou, Additive manufacturing and its societal impact: a literature review, Int. J. Adv. Manuf. Technol. 67 (2013) 1191–1203, https://doi.org/10.1007/s00170-012-4558-5.

[34] M. Javaid, A. Haleem, R.P. Singh, R. Suman, S. Rab, Role of additive manufacturing applications towards environmental sustainability, Adv. Ind. Eng. Polym. Res. 4 (2021) 312–322, https://doi.org/10.1016/J.AIEPR.2021.07.005.

[35] A. Sarbajna, A.G. Rösch, L. Franke, U. Lemmer, M.M. Mallick, Inorganic-based printed thermoelectric materials and devices, Adv. Eng. Mater. 25 (2023) 2200980, https://doi.org/10.1002/ADEM.202200980.

[36] G.M. Guttmann, S. Haroush, Y. Gelbstein, The mechanical properties of inorganic thermoelectric materials: a review on characterization methods and correlations, ChemNanoMat 8 (2022), https://doi.org/10.1002/cnma.202200203.

[37] C. Candolfi, S. El Oualid, B. Lenoir, T. Caillat, Progress and perspectives in thermoelectric generators for waste-heat recovery and space applications, J. Appl. Phys. 134 (2023) 100901, https://doi.org/10.1063/5.0166338/2910452.

[38] J. Shi, X. Chen, W. Wang, H. Chen, A new rapid synthesis of thermoelectric Sb2Te3 ingots using selective laser melting 3D printing, Mater. Sci. Semicond. Process. 123 (2021) 105551, https://doi.org/10.1016/j.mssp.2020.105551 (accessed April 11, 2023).

[39] A. El-Desouky, M. Carter, M. Mahmoudi, A. Elwany, S. Leblanc, Influences of energy density on microstructure and consolidation of selective laser melted bismuth telluride thermoelectric powder, J. Manuf. Process. 25 (2017) 411–417, https://doi.org/10.1016/j.jmapro.2016.12.008.

[40] X.L. Shi, J. Zou, Z.G. Chen, Advanced thermoelectric design: from materials and structures to devices, Chem. Rev. 120 (2020) 7399–7515, https://doi.org/10.1021/acs.chemrev.0c00026.

[41] F. Tohidi, S.G. Holagh, A. Chitsaz, Thermoelectric generators: a comprehensive review of characteristics and applications, Appl. Therm. Eng. 201 (2022) 117793, https://doi.org/10.1016/j.applthermaleng.2021.117793.

[42] P. Sun, B. Wei, J. Zhang, J.M. Tomczak, A.M. Strydom, M. Søndergaard, B. B. Iversen, F. Steglich, Large Seebeck effect by charge-mobility engineering, Nat. Commun. 6 (2015) 1–5, https://doi.org/10.1038/ncomms8475.

[43] S.M. Pourkiaei, M.H. Ahmadi, M. Sadeghzadeh, S. Moosavi, F. Pourfayaz, L. Chen, M.A. Pour Yazdi, R. Kumar, Thermoelectric cooler and thermoelectric generator devices: a review of present and potential applications, modeling and materials, Energy 186 (2019) 115849, https://doi.org/10.1016/j.energy.2019.07.179.

[44] M. Burton, G. Howells, J. Atoyo, M. Carnie, Printed thermoelectrics, Adv. Mater. 34 (2022), https://doi.org/10.1002/adma.202108183.

[45] Y. Du, J. Chen, Q. Meng, Y. Dou, J. Xu, S.Z. Shen, Thermoelectric materials and devices fabricated by additive manufacturing, Vacuum 178 (2020) 109384, https://doi.org/10.1016/j.vacuum.2020.109384.

[46] D. Zhao, G. Tan, A review of thermoelectric cooling: materials, modeling and applications, Appl. Therm. Eng. 66 (2014) 15–24, https://doi.org/10.1016/j.applthermaleng.2014.01.074.

[47] M. Haras, T. Skotnicki, Thermoelectricity for IoT-A review, Nano Energy 54 (2018) 461–476, https://doi.org/10.1016/j.nanoen.2018.10.013.

[48] Z. Soleimani, S. Zoras, B. Ceranic, S. Shahzad, Y. Cui, A review on recent developments of thermoelectric materials for room-temperature applications, Sustain. Energy Technol. Assess. 37 (2020) 100604, https://doi.org/10.1016/J.SETA.2019.100604.

[49] J. Zang, J. Chen, Z. Chen, Y. Li, J. Zhang, T. Song, B. Sun, Printed flexible thermoelectric materials and devices, J. Mater. Chem. A 9 (2021) 19439–19464, https://doi.org/10.1039/D1TA03647E.

[50] J. Qiu, Y. Yan, T. Luo, K. Tang, L. Yao, J. Zhang, M. Zhang, X. Su, G. Tan, H. Xie, M.G. Kanatzidis, C. Uher, X. Tang, 3D printing of highly textured bulk thermoelectric materials: mechanically robust BiSbTe alloys with superior performance, Energy Environ. Sci. 12 (2019) 3106, https://doi.org/10.1039/c9ee02044f.

[51] K. Giri, Y.L. Wang, T.H. Chen, C.H. Chen, Challenges and strategies to optimize the figure of merit: keeping eyes on thermoelectric metamaterials, Mater. Sci. Semicond. Process. 150 (2022) 106944, https://doi.org/10.1016/j.mssp.2022.106944.

[52] Y.M. Poplavko, Metals, Electron. Mater. (2019) 165–220, https://doi.org/10.1016/B978-0-12-815780-0.00005-0.

[53] T.M. Tritt, M.A. Subramanian, Thermoelectric materials, phenomena, and applications: a bird's eye view, MRS Bull. 31 (2006) 188–194, https://doi.org/10.1557/MRS2006.44/METRICS.

[54] W. Liu, Q. Jie, H.S. Kim, Z. Ren, Current progress and future challenges in thermoelectric power generation: from materials to devices, Acta Mater. 87 (2015) 357–376, https://doi.org/10.1016/j.actamat.2014.12.042.

[55] A. Ali, Y. Chen, V. Vasiraju, S. Vaddiraju, Nanowire-Based Thermoelectrics, 2017.

[56] R. Freer, D. Ekren, T. Ghosh, K. Biswas, P. Qiu, S. Wan, L. Chen, S. Han, C. Fu, T. Zhu, A.K.M. Ashiquzzaman Shawon, A. Zevalkink, K. Imasato, G.J. Snyder, M. Ozen, K. Saglik, U. Aydemir, R. Cardoso-Gil, E. Svanidze, R. Funahashi, A. V. Powell, S. Mukherjee, S. Tippireddy, P. Vaqueiro, F. Gascoin, T. Kyratsi, P. Sauerschnig, T. Mori, Key properties of inorganic thermoelectric materials—tables (version 1), J. Phys. Energy 4 (2022) 022002, https://doi.org/10.1088/2515-7655/AC49DC.

[57] H. Wang, C. Yu, Organic thermoelectric materials and devices, Thermoelectr Energy Convers. Theor. Mech. Mater. Devices, Appl. (2021) 347–365, https://doi.org/10.1016/B978-0-12-818535-3.00005-0.

[58] J. Li, A.B. Huckleby, M. Zhang, Polymer-based thermoelectric materials : a review of power factor improving strategies, J. Mater. 8 (2022) 204–220, https://doi.org/10.1016/j.jmat.2021.03.013.

[59] M. Zeng, D. Zavanelli, J. Chen, M. Saeidi-Javash, Y. Du, S. Leblanc, G.J. Snyder, Y. Zhang, Printing thermoelectric inks toward next-generation energy and thermal devices, Chem. Soc. Rev. 51 (2022) 485–512, https://doi.org/10.1039/d1cs00490e.

[60] S. Azam, M.F. Ijaz, S. Azam, M.F. Ijaz, Organic thermoelectric materials, New Mater. Devices Thermoelectr. Power Gener. (2023), https://doi.org/10.5772/INTECHOPEN.1002446.

[61] Y. Hosokawa, K. Tomita, M. Takashiri, Growth of single-crystalline Bi2Te3 hexagonal nanoplates with and without single nanopores during temperature-controlled solvothermal synthesis, Sci. Rep. 91 (9) (2019) 1–7, https://doi.org/10.1038/s41598-019-47356-5.

[62] Y. Pan, J.F. Li, Bismuth telluride, Thermoelectr. Energy Convers. Theor. Mech. Mater. Devices, Appl. (2021) 45–67, https://doi.org/10.1016/B978-0-12-818535-3.00002-5.

[63] C. Uher, Thermoelectric properties of skutterudites, Thermoelectr. Energy Convers. Theor. Mech. Mater. Devices, Appl. (2021) 69–123, https://doi.org/10.1016/B978-0-12-818535-3.00013-X.

[64] J.W.G. Bos, Recent developments in half-Heusler thermoelectric materials, Thermoelectr. Energy Convers. Theor. Mech. Mater. Devices Appl. (2021) 125–142, https://doi.org/10.1016/B978-0-12-818535-3.00014-1.

[65] Y. Yan, H. Ke, J. Yang, C. Uher, X. Tang, Fabrication and thermoelectric properties of n-type CoSb2.85Te0.15 using selective laser melting, ACS Appl. Mater. Interfaces 10 (2018) 13669–13674, https://doi.org/10.1021/acsami.8b01564.

[66] ISO/ASTM, ISO/ASTM 52900:2015, Standard Terminology for Additive Manufacturing– General Principles-Terminology, 2015 https://www.iso.org/standard/69669.html#:~:text=Abstract,into specific fields of application (accessed August 27, 2022).
[67] S.A.M. Tofail, E.P. Koumoulos, A. Bandyopadhyay, S. Bose, L. O'Donoghue, C. Charitidis, Additive manufacturing: scientific and technological challenges, market uptake and opportunities, Mater. Today 21 (2018) 22–37, https://doi.org/10.1016/J.MATTOD.2017.07.001.
[68] S.Y. Liu, H.Q. Li, C.X. Qin, R. Zong, X.Y. Fang, The effect of energy density on texture and mechanical anisotropy in selective laser melted Inconel 718, Mater. Des. 191 (2020) 108642, https://doi.org/10.1016/J.MATDES.2020.108642.
[69] Y. Huang, T.G. Fleming, S.J. Clark, S. Marussi, K. Fezzaa, J. Thiyagalingam, C.L. A. Leung, P.D. Lee, Keyhole fluctuation and pore formation mechanisms during laser powder bed fusion additive manufacturing, Nat. Commun. 131 (13) (2022) 1–11, https://doi.org/10.1038/s41467-022-28694-x.
[70] B. Zhang, Y. Li, Q. Bai, Defect formation mechanisms in selective laser melting: a review, Chinese J. Mech. Eng. 30 (2017) 515–527, https://doi.org/10.1007/S10033-017-0121-5/FIGURES/17.
[71] L. Mugwagwa, I. Yadroitsava, N.W. Makoana, I. Yadroitsev, Residual stress in laser powder bed fusion, Fundam. Laser Powder Bed Fusion Met. (2021) 245–276, https://doi.org/10.1016/B978-0-12-824090-8.00014-7.
[72] A. Baroutaji, A. Arjunan, J. Beal, J. Robinson, J. Coroado, The influence of atmospheric oxygen content on the mechanical properties of selectively laser melted AlSi10Mg TPMS-based lattice, Mater 16 (2023) 430, https://doi.org/10.3390/MA16010430.
[73] A. Baroutaji, A. Arjunan, M. Stanford, J. Robinson, A.G. Olabi, Deformation and energy absorption of additively manufactured functionally graded thickness thin-walled circular tubes under lateral crushing, Eng. Struct. 226 (2021) 111324, https://doi.org/10.1016/J.ENGSTRUCT.2020.111324.
[74] H. Wu, B. Hu, N. Tian, Q. Zheng, Preparation of β-FeSi2 thermoelectric material by laser sintering, Mater. Lett. 65 (2011) 2877–2879.
[75] Y. Kinemuchi, M. Mikami, I. Terasaki, W. Shin, Rapid synthesis of thermoelectric compounds by laser melting, Mater. Des. 106 (2016) 30–36. https://doi.org/10.1016/j.matdes.2016.05.093, (accessed April 5 2023).
[76] A. El-Desouky, M. Carter, M.A. Andre, P.M. Bardet, S. Leblanc, Rapid Processing and Assembly of Semiconductor Thermoelectric Materials for Energy Conversion Devices, 2016, https://doi.org/10.1016/j.matlet.2016.07.152.
[77] T. Le Chen, C. Luo, Y.G. Yan, J.H. Yang, Q.J. Zhang, C. Uher, X.F. Tang, Rapid fabrication and thermoelectric performance of SnTe via non-equilibrium laser 3D printing, Rare Metals 37 (2018) 300–307, https://doi.org/10.1007/S12598-018-1019-9/FIGURES/5.
[78] M.J. Carter, A. El-Desouky, M.A. Andre, P. Bardet, S. LeBlanc, Pulsed laser melting of bismuth telluride thermoelectric materials, J. Manuf. Process. 43 (2019) 35–46, https://doi.org/10.1016/J.JMAPRO.2019.04.021.
[79] H. Zhang, D. Hobbis, G.S. Nolas, S. Leblanc, Laser additive manufacturing of powdered bismuth telluride, J. Mater. Res. 33 (2018) 4031–4039, https://doi.org/10.1557/JMR.2018.390.
[80] H. Zhang, S. LeBlanc, Laser additive manufacturing process development for Bismuth telluride thermoelectric material, J. Mater. Eng. Perform. 31 (2022) 6196–6204, https://doi.org/10.1007/S11665-022-07084-W/FIGURES/7.
[81] Y. Mao, Y. Yan, K. Wu, H. Xie, Z. Xiu, J. Yang, Q. Zhang, C. Uher, X. Tang, Non-equilibrium synthesis and characterization of n-type Bi2Te2.7Se0.3 thermoelectric material prepared by rapid laser melting and solidification, RSC Adv. 7 (2017) 21439–21445, https://doi.org/10.1039/C7RA02677C.
[82] K. Wu, Y. Yan, J. Zhang, Y. Mao, H. Xie, J. Yang, Q. Zhang, C. Uher, X. Tang, Preparation of n-type Bi2Te3 thermoelectric materials by non-contact dispenser printing combined with selective laser melting, Phys. Status Solidi Rapid Res. Lett. 11 (2017) 1700067, https://doi.org/10.1002/PSSR.201700067.
[83] R. Welch, D. Hobbis, A.J. Birnbaum, G. Nolas, S. LeBlanc, Nano- and Micro-structures formed during laser processing of selenium doped Bismuth telluride, Adv. Mater. Interfaces 8 (2021), https://doi.org/10.1002/ADMI.202100185.
[84] J.Y. Yang, W. Zhu, H. Li, X. Cheng, Q. Zheng, H. Lia, X. Cheng, X. Xiong, L. Zhu, G. Wang, D. Liu, Q. Zhang, W. Feng, Microstructure and properties of n-type Bi2Te3-based thermoelectric material fabricated by selective laser sintering, Mater. Res. Express 7 (2020) 066504, https://doi.org/10.1088/2053-1591/AB81BE.
[85] J. Shi, H. Chen, S. Jia, W. Wang, 3D Printing Fabrication of Porous Bismuth Antimony telluride and Study of the Thermoelectric Properties, 2018, https://doi.org/10.1016/j.jmapro.2018.11.001.
[86] F. Chen, R. Liu, Z. Yao, Y. Xing, S. Bai, L. Chen, Scanning laser melting for rapid and massive fabrication of filled skutterudites with high thermoelectric performance, J. Mater. Chem. A 6 (2018) 6772–6779, https://doi.org/10.1039/C8TA01504J.
[87] H. Zhang, S. Wang, P.J. Taylor, J. Yang, S. LeBlanc, Selective laser melting of half-Heusler thermoelectric materials, in: Proc. Vol. 10663, Energy Harvest. Storage Mater. Devices, Appl. VIII;106630B, SPIE, 2018, pp. 10–17, https://doi.org/10.1117/12.2306099.
[88] Y. Yan, W. Geng, J. Qiu, H. Ke, C. Luo, J. Yang, C. Uher, X. Tang, Thermoelectric properties of n-type ZrNiSn prepared by rapid non-equilibrium laser processing, RSC Adv. 8 (2018) 15796–15803, https://doi.org/10.1039/C8RA00992A.
[89] Y. Thimont, L. Presmanes, V. Baylac, P. Tailhades, D. Berthebaud, F. Gascoin, Thermoelectric higher manganese silicide: synthetized, sintered and shaped simultaneously by selective laser sintering/melting additive manufacturing technique, Mater. Lett. 214 (2018) 236–239.
[90] Z. Sun, X. Tan, S. Beng Tor, W. Yee Yeong, S.B. Tor, W.Y. Yeong, Selective laser melting of stainless steel 316L with low porosity and high build rates, Mater. Des. 104 (2016) 197–204, https://doi.org/10.1016/j.matdes.2016.05.035 (accessed September 17, 2023).
[91] A. Baroutaji, A. Arjunan, G. Singh, J. Robinson, Crushing and energy absorption properties of additively manufactured concave thin-walled tubes, Res. Eng. Des. 14 (2022) 100424, https://doi.org/10.1016/J.RINENG.2022.100424.
[92] A. Arjunan, M. Demetriou, A. Baroutaji, C. Wang, Mechanical performance of highly permeable laser melted Ti6Al4V bone scaffolds, J. Mech. Behav. Biomed. Mater. (2020), https://doi.org/10.1016/j.jmbbm.2019.103517.
[93] C.T. Wanniarachchi, A. Arjunan, A. Baroutaji, M. Singh, 3D printing customised stiffness-matched meta-biomaterial with near-zero auxeticity for load-bearing tissue repair, Bioprinting 33 (2023) e00292, https://doi.org/10.1016/J.BPRINT.2023.E00292.
[94] J. Robinson, A. Arjunan, A. Baroutaji, M. Stanford, Mechanical and thermal performance of additively manufactured copper, silver, and copper-silver alloys, Proc. Inst. Mech. Eng. Part L J. Mater. Des. Appl. (2021), https://doi.org/10.1177/14644207211040929.
[95] J. Robinson, S.P. Munagala, A. Arjunan, N. Simpson, R. Jones, A. Baroutaji, L. T. Govindaraman, I. Lyall, Electrical conductivity of additively manufactured copper and silver for electrical winding applications, Mater 15 (2022) 7563, https://doi.org/10.3390/MA15217563.
[96] C. Luo, J. Qiu, Y. Yan, J. Yang, C. Uher, X. Tang, Finite element analysis of temperature and stress fields during the selective laser melting process of thermoelectric SnTe, J. Mater. Process. Technol. 261 (2018) 74–85, https://doi.org/10.1016/j.jmatprotec.2018.06.001.
[97] G. Tan, L.D. Zhao, M.G. Kanatzidis, Rationally designing high-performance bulk thermoelectric materials, Chem. Rev. 116 (2016) 12123–12149, https://doi.org/10.1021/acs.chemrev.6b00255.
[98] Y. Wu, K. Sun, S. Yu, L. Zuo, Modeling the selective laser melting-based additive manufacturing of thermoelectric powders, Addit. Manuf. 37 (2021) 101666, https://doi.org/10.1016/j.addma.2020.101666.
[99] F.D.C. Siacor, Q. Chen, J.Y. Zhao, L. Han, A.D. Valino, E.B. Taboada, E. B. Caldona, R.C. Advincula, On the additive manufacturing (3D printing) of viscoelastic materials and flow behavior: from composites to food manufacturing, Addit. Manuf. 45 (2021) 102043, https://doi.org/10.1016/j.addma.2021.102043.
[100] Y. Eom, F. Kim, S. Eun Yang, A. Phys Lett, J. Sung Son, H. Gi Chae, Rheological design of 3D printable all-inorganic inks using BiSbTe-based thermoelectric materials, J. Appl. Phys. 63 (2019) 291–304, https://doi.org/10.1122/1.5058078.
[101] J. Plog, Y. Jiang, Y. Pan, A.L. Yarin, Electrostatically-assisted direct ink writing for additive manufacturing, Addit. Manuf. 39 (2021) 101644, https://doi.org/10.1016/j.addma.2020.101644.
[102] M.A.S.R. Saadi, A. Maguire, N.T. Pottackal, M. Shajedul Hoque Thakur, M. Md Ikram, A. John Hart, P.M. Ajayan, M.M. Rahman, A. Maguire, N.T. Pottackal, M.S.H. Thakur, P.M. Ajayan, M.M. Rahman, M. Md Ikram, A.J. Hart, Direct ink writing: a 3D printing technology for diverse materials, Adv. Mater. 34 (2022) 2108855, https://doi.org/10.1002/ADMA.202108855.
[103] A. Shahzad, I. Lazoglu, Direct ink writing (DIW) of structural and functional ceramics: recent achievements and future challenges, Compos. Part B Eng. 225 (2021) 109249, https://doi.org/10.1016/j.compositesb.2021.109249.
[104] D. Madan, A. Chen, P.K. Wright, J.W. Evans, Dispenser printed composite thermoelectric thick films for thermoelectric generator applications, J. Appl. Phys. 109 (2011) 34904, https://doi.org/10.1063/1.3544501.
[105] A. Chen, D. Madan, P.K. Wright, J.W. Evans, Dispenser-printed planar thick-film thermoelectric energy generators, J. Micromech. Microeng. 21 (2011), https://doi.org/10.1088/0960-1317/21/10/104006.
[106] Z. Cao, J.J. Shi, R.N. Torah, M.J. Tudor, S.P. Beeby, All dispenser printed flexible 3D structured thermoelectric generators, J. Phys. Conf. Ser. 660 (2015) 6–11, https://doi.org/10.1088/1742-6596/660/1/012096.
[107] M. Shakeel, K. Rehman, S. Ahmad, M. Amin, N. Iqbal, A. Khan, A low-cost printed organic thermoelectric generator for low-temperature energy harvesting, Renew. Energy 167 (2021) 853–860, https://doi.org/10.1016/j.renene.2020.11.158.
[108] Y. Du, J. Chen, Q. Meng, J. Xu, J. Lu, B. Paul, P. Eklund, Flexible thermoelectric double-layer inorganic/organic composites synthesized by additive manufacturing, Adv. Electron. Mater. 6 (2020) 1–8, https://doi.org/10.1002/aelm.202000214.
[109] Y. Du, J. Chen, X. Liu, C. Lu, J. Xu, B. Paul, P. Eklund, Flexible n-type tungsten carbide/polylactic acid thermoelectric composites fabricated by additive manufacturing, Coatings 8 (2018) 25, https://doi.org/10.3390/COATINGS8010025.
[110] Y. Du, J. Chen, Q. Meng, J. Xu, B. Paul, P. Eklund, Flexible ternary carbon black/Bi2Te3 based alloy/polylactic acid thermoelectric composites fabricated by additive manufacturing, J. Mater. 6 (2020) 293–299, https://doi.org/10.1016/j.jmat.2020.02.010.
[111] S. Hwang, D. Jang, B. Lee, Y.S. Ryu, J. Kwak, H. Kim, S. Chung, All direct ink writing of 3D compliant carbon thermoelectric generators for high-energy conversion efficiency, Adv. Energy Mater. (2023) 2204171, https://doi.org/10.1002/aenm.202204171.
[112] S. Kee, M.A. Haque, D. Corzo, H.N. Alshareef, D. Baran, Self-healing and stretchable 3D-printed organic thermoelectrics, Adv. Funct. Mater. 29 (2019), https://doi.org/10.1002/ADFM.201905426.
[113] F. Kim, B. Kwon, Y. Eom, J.E. Lee, S. Park, S. Jo, S.H. Park, B.S. Kim, H.J. Im, M. H. Lee, T.S. Min, K.T. Kim, H.G. Chae, W.P. King, J.S. Son, 3D printing of shape-conformable thermoelectric materials using all-inorganic Bi2Te3-based inks, Nat. Energy 34 (3) (2018) 301–309, https://doi.org/10.1038/s41560-017-0071-2.

[114] F. Kim, S.E. Yang, H. Ju, S. Choo, J. Lee, G. Kim, S. Ho Jung, S. Kim, C. Cha, K. T. Kim, S. Ahn, H.G. Chae, J.S. Son, Direct ink writing of three-dimensional thermoelectric microarchitectures, Nat. Electron. 48 (4) (2021) 579–587, https://doi.org/10.1038/s41928-021-00622-9.

[115] Z. Wang, W. Cui, H. Yuan, X. Kang, Z. Zheng, L. Chen, Q. Hu, W. Qiu, J. Tang, X. Cui, Direct ink writing of high-performance bi 2 Te 3-based thermoelectric materials using quasi-inorganic inks and interface engineering, J. Mater. Chem. A 10 (2022) 12921, https://doi.org/10.1039/d2ta02289c.

[116] Z. Wang, W. Cui, H. Yuan, X. Kang, Z. Zheng, W. Qiu, Q. Hu, J. Tang, X. Cui, Direct ink writing of Bi2Te 3-based thermoelectric materials induced by rheological design, Mater. Today Energy 31 (2022) 101206, https://doi.org/10.1016/j.mtener.2022.101206.

[117] A. Elkaseer, K.J. Chen, J.C. Janhsen, O. Refle, V. Hagenmeyer, S.G. Scholz, Material jetting for advanced applications: a state-of-the-art review, gaps and future directions, Addit. Manuf. 60 (2022) 103270, https://doi.org/10.1016/j.addma.2022.103270.

[118] F. Liravi, M. Salarian, C. Dal Castel, L. Simon, E. Toyserkani, High-speed material jetting additive manufacturing of silicone structures: mechanical characterization, Prog. Addit. Manuf. 4 (2019) 479–495, https://doi.org/10.1007/S40964-019-00097-3/FIGURES/12.

[119] M. Heidari-Rarani, M. Rafiee-Afarani, A.M. Zahedi, Mechanical characterization of FDM 3D printing of continuous carbon fiber reinforced PLA composites, Compos. Part B Eng. 175 (2019) 107147, https://doi.org/10.1016/j.compositesb.2019.107147.

[120] D. Popescu, A. Zapciu, C. Amza, F. Baciu, R. Marinescu, FDM process parameters influence over the mechanical properties of polymer specimens: a review, Polym. Test. 69 (2018) 157–166, https://doi.org/10.1016/j.polymertesting.2018.05.020.

[121] A. Cano-Vicent, M.M. Tambuwala, S.S. Hassan, D. Barh, A.A.A. Aljabali, M. Birkett, A. Arjunan, Á. Serrano-Aroca, Fused deposition modelling: current status, methodology, applications and future prospects, Addit. Manuf. 47 (2021), https://doi.org/10.1016/j.addma.2021.102378.

[122] I. Gibson, D. Rosen, B. Stucker, Additive Manufacturing Technologies: 3D Printing, Rapid Prototyping, and Direct Digital Manufacturing, Second edition, 2015, pp. 1–498, https://doi.org/10.1007/978-1-4939-2113-3/COVER.

[123] A. Baroutaji, A. Arjunan, J. Robinsion, M. Ramadan, M.A. Abdelkareem, A.-G. Olabi, Metamaterial for crashworthiness applications, Encycl Smart Mater. (2022) 57–69, https://doi.org/10.1016/B978-0-12-815732-9.00092-9.

[124] Y.Y. Aw, C.K. Yeoh, M.A. Idris, P.L. Teh, K.A. Hamzah, S.A. Sazali, Effect of printing parameters on tensile, dynamic mechanical, and thermoelectric properties of FDM 3D printed CABS/ZnO composites, Mater 11 (2018) 466, https://doi.org/10.3390/MA11040466.

[125] J. Wang, H. Li, R. Liu, L. Li, Y.H. Lin, C.W. Nan, Thermoelectric and mechanical properties of PLA/Bi0·5Sb1·5Te3 composite wires used for 3D printing, Compos. Sci. Technol. 157 (2018) 1–9, https://doi.org/10.1016/j.compscitech.2018.01.013.

[126] Z.G. Chen, X. Shi, L.D. Zhao, J. Zou, High-performance SnSe thermoelectric materials: progress and future challenge, Prog. Mater. Sci. 97 (2018) 283–346, https://doi.org/10.1016/j.pmatsci.2018.04.005.

[127] D. Zhang, W.Y.S. Lim, S.S.F. Duran, X.J. Loh, A. Suwardi, Additive manufacturing of thermoelectrics: emerging trends and outlook, ACS Energy Lett. 7 (2022) 720–735, https://doi.org/10.1021/ACSENERGYLETT.1C02553.

[128] W.Z. Tan, C.H. Koo, W.J. Lau, W.C. Chong, J.Y. Tey, Recent Advances in 3D Printed Membranes for Water Applications, in: 60 Years Loeb-Sourirajan Membr. Princ. New Mater. Model. Charact. Appl., INC, 2022, pp. 71–96, https://doi.org/10.1016/B978-0-323-89977-2.00012-9.

[129] A. Bagheri, J. Jin, Photopolymerization in 3D printing, ACS Appl. Polym. Mater. 1 (2019) 593–611, https://doi.org/10.1021/acsapm.8b00165.

[130] J. An, Polymer materials for additive manufacturing, INC (2022), https://doi.org/10.1016/B978-0-323-95062-6.00011-5.

[131] A. Davoudinejad, Vat Photopolymerization Methods in Additive Manufacturing, Elsevier Inc., 2021, https://doi.org/10.1016/B978-0-12-818411-0.00007-0.

[132] A. Neagu, 3D Bioprinting Techniques, 2023, https://doi.org/10.1016/b978-0-12-818653-4.00004-8.

[133] J.R. Tumbleston, D. Shirvanyants, N. Ermoshkin, R. Janusziewicz, A.R. Johnson, D. Kelly, K. Chen, R. Pinschmidt, J.P. Rolland, A. Ermoshkin, E.T. Samulski, J. M. DeSimone, Continuous liquid interface production of 3D objects, Science 347 (2015) 1349–1352, https://doi.org/10.1126/sciadv.abq3917.

[134] M. He, Y. Zhao, B. Wang, Q. Xi, J. Zhou, Z. Liang, 3D printing fabrication of amorphous thermoelectric materials with ultralow thermal conductivity, Small 11 (2015) 5889–5894, https://doi.org/10.1002/SMLL.201502153.